Defence Research and Development Canada | Recherche et développement pour la défense Canada

DEFENCE R&D DÉFENSE

# End-to-End Statistical World Representations:

*Terrain Mapping to Traversability Analysis*

G.S. Broten
J.A. Collier

D.J. Mackay
S.P. Monckton

B.L. Digney
Defence R&D Canada – Suffield

**Defence R&D Canada**
Technical Report
DRDC Suffield TR 2013-060
November 2013

Canada

# End-to-End Statistical World Representations:

*Terrain Mapping to Traversability Analysis*

G.S. Broten
J.A. Collier

D.J. Mackay
S.P. Monckton

B.L. Digney
Defence R&D Canada – Suffield

**Defence R&D Canada – Suffield**

Technical Report
DRDC Suffield TR 2013-060
November 2013

# Abstract

Robot navigation requires reliable perception that generates an appropriate world representation. This is especially true for outdoor, unstructured or semi-structured environments where impediments to traversal are more complex than simple insurmountable obstacles. Such environments include negative features, such as ditches, as well as positive features in the form of sloping rises, that may constitute obstacles to traversal. These features must be captured by the world representation in a manner that properly handles the uncertainty associated with range data and the vehicle pose. An analysis of this representation can then extract traversable and non-traversable regions. Finally, this processing must proceed in near real-time in order to allow the robot to travel at reasonable speeds. This paper presents a statistical approach that starts with a 2.5D terrain map, follows through to the traversability analysis, and continues to the ancillary global terrain and traversability representations. At all stages the data's statistical relevance is carried forward and incorporated into the analysis. This technique has been verified using simulations and heavily exercised on a physical robot under real world conditions. These experiments have revealed that the proposed approach performs well, producing both terrain and traversability maps that adequately portray their environment.

# Résumé

La navigation par robot exige une perception fiable selon laquelle une représentation appropriée du monde est produite. Cela est particulièrement vrai pour les environnements extérieurs, non structurés ou semi-structurés où les entraves au déplacement sont plus complexes que de simples obstacles insurmontables. Ces environnements comportent des particularités négatives, comme des fossés, ainsi que des particularités positives se présentant sous la forme de pentes montantes, qui peuvent gêner le déplacement. Ces particularités doivent être saisies lors de la représentation du monde d'une manière qui permette de gérer l'incertitude associée aux données télémétriques et à la pose d'un véhicule. Une analyse de cette représentation permet ensuite d'extraire les régions où des obstacles gênent le déplacement et où ce dernier peut se faire librement. Enfin, ce traitement doit se faire en temps quasi-réel afin de que le robot puisse se déplacer à des vitesses raisonnables. Le présent document décrit une approche statistique établie d'après une carte topographique 2.5D; il traite ensuite de l'analyse des entraves au déplacement et se poursuit par des représentations auxiliaires globales concernant le terrain et le déplacement sans gêne. À toutes les étapes, la pertinence des données sur le plan statistique est reprise et intégrée à l'analyse. Cette technique a été vérifiée au moyen de simulations et a été mise à l'épreuve de manière intensive sur un robot physique dans des conditions du monde réel. Ces expériences ont révélé que l'approche proposée fonctionne bien; elle produit des cartes du terrain et des entraves au déplacement qui décrivent de manière adéquate l'environnement.

This page intentionally left blank.

# Executive summary

## End-to-End Statistical World Representations

G.S. Broten, J.A. Collier, D.J. Mackay, S.P. Monckton, B.L. Digney;
DRDC Suffield TR 2013-060; Defence R&D Canada – Suffield; November 2013.

Background: For a robot traversing semi-structured environments a local world representation is a crucial component of an obstacle and hazard avoidance capability. Additionally, a global world representation, constructed as the robot explores its environment, is also desirable as it enables long range path planning. The key challenge is to represent unstructured terrain in a manner that captures its uncertainty, yet is still amenable to real-time or near real-time analysis. This paper exploits range sensor data's statistical properties from its acquisition through all aspects of its anal-ysis. Under this end-to-end approach, all algorithms incorporate the data quality, providing probabilistic estimates of world representation.

Principal Results: This systematic statistical approach has been tested extensively via simulations and under real world conditions. These experiments have revealed a robust implementation that reliably and accurately represents the environment. Cross validation experiments highlighted the statistical implementation's superior performance over an alternative heuristic based approach.

Significance of Results: In simulation where the range data was corrupted by a spe-cific amount, the probabilistic traversability approach was an improvement over the previous purely heuristic approach. With real world data the probabilistic traversabil-ity map reliably identified impediments to traversal.

Future Work: This statistical approach is amenable to other types of traversability analysis. Vehicle roll over is another significant hazard where, traditionally, purely heuristic approaches have been the norm. This statistical approach has been adapted to predict the roll over hazard, but experiments to quantify its performance have yet to be conducted.

Additionally, it would be highly desirable to compare the presented technique's performance against other traversability implementations, especially the probabilistic technique used by the Stanley UGV. Unfortunately such comparisons are difficult to perform given that this would require an independent implementation of the "probabilistic terrain analysis" approach, which is not a simple and straightforward task.

# Sommaire


## End-to-End Statistical World Representations

G.S. Broten, J.A. Collier, D.J. Mackay, S.P. Monckton, B.L. Digney ; DRDC Suffield TR 2013-060 ; Défense R et D Canada – Suffield ; novembre 2013.

Contexte : Lorsqu'un robot se déplace dans des environnements semi-structurés, il est crucial de pouvoir disposer d'une représentation locale du monde dans lequel il se trouve afin qu'il puisse éviter les obstacles et les dangers présents. De plus, il est aussi souhaitable d'obtenir une représentation globale du monde, construite à mesure que le robot explore son environnement, car cela permet de planifier le déplacement sur une longue distance. Le défi principal est de représenter le terrain non structuré d'une manière qui permette de prendre en compte l'incertitude, et cela se prête par ailleurs à une analyse en temps réel ou quasi-réel. Le présent document exploite les propriétés statistiques en regard des données télémétriques d'un capteur, et ce, depuis l'acquisition de ces dernières jusqu'à une analyse de tous leurs aspects. Selon cette approche de bout en bout, tous les algorithmes intègrent la qualité des données, donnant lieu à des estimations probabilistes de la représentation du monde.

Résultats principaux : Cette approche statistique systématique a été mise à l'épreuve de manière intensive au moyen de simulations et dans des conditions du monde réel. Ces expériences ont révélé que cette approche pouvait donner lieu à une solide mise en œuvre afin de permettre de représenter de manière fiable et précise l'environnement. Des expériences de validation croisée démontrent que la mise en œuvre par des moyens statistiques produit des performances supérieures à celles obtenues selon une autre approche heuristique.

Importance des résultats : Dans une simulation où les données télémétriques ont été corrompues dans une certaine mesure, l'approche probabiliste liée aux entraves au déplacement a donné un meilleur résultat que l'approche purement heuristique précédente. En présence de données du monde réel, la carte probabiliste des entraves au déplacement a permis d'identifier de manière fiable ces dernières.

Travaux futurs : Cette approche statistique se prête à d'autres types d'analyse liée aux entraves au déplacement. Le renversement d'un véhicule constitue un autre risque important où, traditionnellement, l'on a recouru en règle générale à des approches purement heuristiques. Cette approche statistique a été adaptée afin de prédire le risque de renversement d'un véhicule, mais il reste à mener des expériences visant à quantifier les performances de celle-ci.

De plus, il serait fortement souhaitable de comparer les performances de la technique présentée à celles d’autres activités mises en œuvre relativement à l’analyse des entraves au déplacement, en particulier la technique probabiliste utilisée par le VTSP Stanley. Malheureusement, de telles comparaisons restent difficiles à concrétiser, car cela nécessiterait une mise en œuvre indépendante de l’approche liée à l’« analyse probabiliste du terrain », ce qui n’est une tâche ni simple ni facile.

# Table of contents

# List of figures

# List of tables

This page left intentionally blank

# 1 Introduction

Outdoor, unstructured or semi-structured environments feature man made obstacle forms such as buildings, vehicles and curbs, along with impediments to traversal such as rocks, berms, ditches, and vegetation. For a robot traversing these types of environments a local world representation is a crucial component of an obstacle and hazard avoidance capability. Additionally, a global world representation, constructed as the robot explores its environment, is also desirable as it enables long range path planning. The key challenge is to represent unstructured terrain in a manner that captures its uncertainty, yet is still amenable to real-time or near real-time analysis.

A common first stage in converting sensor data into a world representation is the terrain map. The terrain map represents the environment around the vehicle through a 2.5D elevation grid, where each grid element is uniform in size. Grid elements with valid data encode the terrain elevation and grid elements without data are marked as unknown terrain. The terrain map is a simple world representation that can easily be analysed in near real-time, thus allowing obstacles to be detected. Given the terrain map's geometric-based representation it requires sensory data that samples the environment's geometry. Laser rangefinders, time-of-flight cameras and stereo vision are common sensors used to provide data. Before the advent of high density data sources, the sampling of the environment was often sparse, hence providing limited opportunities for a statistical representation. Stereo vision can provide dense data sets and has been used extensively in space rover implementations where weight and power consumption are important considerations. Unfortunately it suffers from common camera issues such as a limited field of view, sensitivity to lighting conditions and a non-linear error associated with the range determination. On the other hand, laser rangefinders are lighting invariant and have a small, consistent range error, thus they have attained a significant level of acceptance for outdoor applications. Early lasers were only capable of low data densities that sparsely sampled the environment, even if deployed as multiple instances. High density laser rangefinders, such as the Velodyne HD Laser, provide data densities comparable to stereo vision and 360° of coverage. Regardless of the originating sensor, dense data sources provide an opportunity to construct a local terrain map where the underlying data's statistical properties are meaningful.

The terrain map is an intermediate world representation that is not directly usable in the obstacle avoidance problem. Analyzing a terrain map for traversability produces a grid map of traversable, non-traversable and unknown spaces. In general, for this type of traversability analysis, obstacle detection is just one of a number of traversal impediments. Other impediments include a roughness hazard, pitch hazard and border hazard. Obstacle detection is commonly implemented as a thresholded step hazard, which determines the maximum height difference between any pair of cells in a patch. Such a heuristic approach, based upon rigid thresholds, doesn't take advantage of the statistical properties of the source terrain and provides the same conclusions regardless of the data's *goodness*. Using a statistical approach, the data's quality becomes an intrinsic part of the obstacle prediction process. This in turn leads to a more reliable obstacle detection scheme.

The main contribution of this paper is a systematic implementation that exploits the data's statistical properties from its acquisition through all aspects of its analysis. Under this end-to-end approach, all algorithms incorporate the data quality, providing probabilistic estimates of world representation. The terrain map captures the statistical significance of the underlying range data. The traversability map estimates the probability of an obstacle. Additionally, the global traversability map statistically fuses together traverse map patches that have been acquired at different times. This statistical approach is enabled by this paper's second contribution; a method of estimating the variance associated with the acquired range data. The estimated elevation variance is shown to be both a function of the range and vehicle's orientation. This systematic statistical approach has been tested extensively via simulations and under real world conditions. These experiments have revealed a robust implementation that reliably and accurately represents the environment. Cross validation experiments highlighted the statistical implementation's superior performance over an alternative heuristic based approach.

This paper is divided into 5 sections. Section 2 broadly reviews previous research into world representations, including terrain maps, traversability maps, and other approaches to detecting obstacles. The proposed end-to-end statistical implementation is presented in Section 3. This includes a theoretical derivation of the elevation variance, a description of the statistical terrain map, and details on the probabilistic approach for constructing the traversability, along with the global traversability map implementation. The results of experiments, conducted in simulations and in the real world, are presented in Section 4. These experiments include cross validation comparisons to other techniques, where applicable. Finally, conclusions are presented in Section 5.

# 2 Related Work

A robotic vehicle that deliberatively plans traversal in a world containing obstacles, must sense its world and create some type of world representation[1]. Even SRI's Shakey and Stanford's cart, the grandfathers of mobile robotic platforms, featured camera based perceptual systems that provided a rudimentary world representation [2, 3]. Another contemporary, the JPL cart, used stereo vision and a laser rangefinder to create a grid based traversability map to represent the terrain surface [4]. By the 1980's sonars provided data to create a grid map representation where elements were defined as empty or occupied [5], and drove the virtual force field [6] and its descendant the vector field histogram [7]. With advances in technology and computational power, higher fidelity sensors, including stereo vision and laser rangefinders, were adopted by robotics researchers and their theoretical statistical properties were investigated [8, 9]. Although stereo vision offers many advantages such as high data densities, a non-emmisive nature, a compact size and low power requirements [10], the active laser rangefinder has proven more popular for outdoor environments. The performance of the popular SICK laser rangefinder has been extensively studied [11], though its low data densities have often forced researchers to use a ganged approach to ensure adequate terrain coverage [12]. In response to both low data densities and the experiences of the DARPA Grand Challenges, manufactures developed *high definition* (HD) lasers that can sample terrain at high data densities. The most significant development, the Velodyne HD Laser, was instrumental on the vehicle that won the DARPA Urban Challenge in 2007 [13]. Unfortunately high density lasers, such as the Ibeo and Velodyne, are physically large and power intensive, thus are not suitable for smaller robotic platforms. Time-of-flight cameras providing high data rates while preserving a compact size could also be attractive alternatives in such situations [14].

Regardless of the sensor, range data's importance lies in its utility in detecting obstacles. To that purpose the occupancy grid has become the dominant paradigm for environmental modeling in mobile robotics [15]. From the classical occupancy grid [16] to current day implementations, the occupancy grid is an enabler of robot navigation capabilities such as localization, path planning and obstacle avoidance. The occupancy grid implementation can take on numerous forms and the merits of differing techniques have been investigated [17].

Although occupancy grids are of utility in structured environments, they are not directly applicable where the shape and form of the terrain may itself constitute an obstacle. In contrast to structured environments where obstacles occupy vertical spaces in an assumed flat world, such structural expectations are not available in unstructured/semi-structured outdoor environments [18]. In such situations a 2.5D terrain map or digital elevation map is more appropriate. A terrain map represents the environment through a 2.5D elevation grid, where elements with valid data encode the terrain elevation and elements without data are marked as unknown terrain. Early research at Carnegie Mellon University relied upon the ERIM laser rangefinder, providing 64 rows by 256 columns of range value, to construct a *snapshot* terrain map [19]. Given the poor pose estimation, available at that time, much effort was expended on merging successive *snapshot* maps into a single representation [20, 21, 22]. With the advent of adequate processing power, the terrain map took its modern form as real-time, wrappable and scrollable region, as succinctly described by Kelly and Stenz [23].

Analysing the terrain map for significant surface changes yields a traversability map

[24, 25]. The Ranger algorithm, an early implementation of this traversability mapping [26], has spawned descendants such as the Morphin algorithm [27] and a NASA implementation called GESTALT [28, 29]. In general, for these types of traversability analysis implementations, obstacle detection is just one of a number of traversal impediments. Other impediments include a roughness hazard, pitch hazard and border hazard. Obstacle detection is commonly implemented as a thresholded step hazard, which determines the maximum height difference between any pair of cells in a patch. Heuristic approaches, based upon rigid thresholds, don't take advantage of the statistical properties of the source terrain, thus provide the same conclusions regardless of the data *goodness*. Additionally, a heuristic implementation requires *manual* tuning whenever the platform or environment changes.

In contrast to the world representation and subsequent traversability analysis paradigm, it is possible to directly detect obstacles in the laser point cloud. A variety of approaches have been implemented including heuristics, classifiers, and statistical implementations. The heuristic approach, similar to traversability analysis, uses predefined thresholds and, hence, suffers from similar limitations [30, 31]. Classification techniques automatically group terrain with similar qualities [32, 33] but the significance of this grouping requires human intervention in terms of data labeling, which is itself a difficult problem [34]. Stanley, the unmanned vehicle that won the Second DARPA Grand Challenge, addressed the obstacle detection problem from a systematic, probabilistic approach [12]. This technique does not create a statistical terrain map, but instead analyzes the raw rangefinder point clouds in order to determine the presence of an obstacle. Thrun et al. recognized that small errors in the vehicle's roll/pitch estimation could lead to significant terrain classification error. Their key insight was that the classification error was strongly correlated with the elapsed time between the two rangefinder scans used in the classification. To counteract this problem, Stanley used a first-order Markov model to track the drift in pose estimation over time [35]. Hence, the test for the presence of an obstacle became a probabilistic test that was distributed normally with a variance that scaled linearly with the time difference between data samples. The Markov model possesses a number of unknown parameters, such as the threshold height and the statistical acceptance probability threshold that were optimized using a discriminative learning algorithm.

# 3 Terrain Mapping for Unstructured Environments

Building a world representation from sensors mounted on a moving platform, poses unique and difficult problems. Sensory data of varying quality, from differing poses, must be integrated into a single coherent representation. Unstructured environments impose additional burdens as the rough terrain causes the platform to roll and pitch unpredictably. The impact of the platform's pose on the acquired range data must be understood and modeled in order to maximize the utility of the world representation.

## 3.1 Pose and Range Data Relationship

The 2.5D terrain map represents the world as an elevation for each grid element within the map. The $(x, y, z)$ components are a function of both the vehicle's pose and the measured range provided by a ranging sensor, as show in Figure 1.

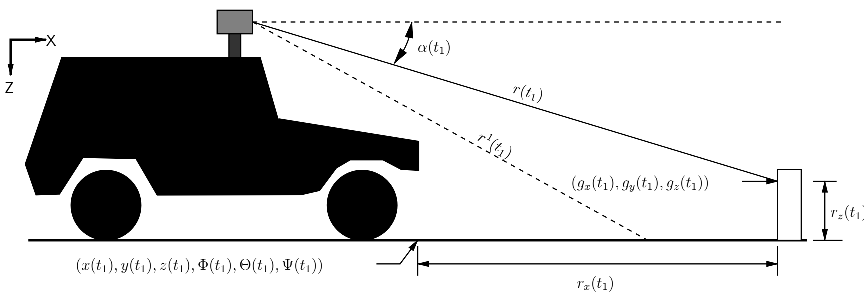


(a) Vehicle at Time $t_1$

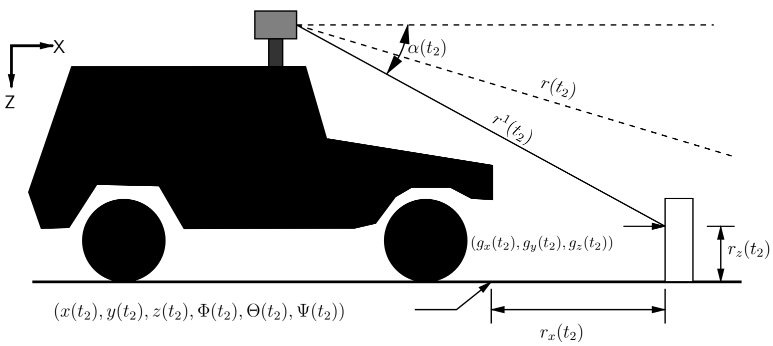


(b) Vehicle at Time $t_2$

***Figure 1:*** *Converting Range to an Elevation in a Terrain Map*

For a vehicle of position $(x(t_1), y(t_1), z(t_1))$ the grid element $(g_x(t), g_y(t), g_z(t))$ is a function of the orientation, $(\Phi(t_1), \Theta(t_1), \Psi(t_1))$ with $\Phi$ as roll, $\Theta$ as pitch and $\Psi$ as yaw, and the measured range, $r(t_1)$, at a projected angle of $\alpha(t_1)$, as shown in Figure 1 (a). As the vehicle moves to a new position, $(x(t_2), y(t_2), z(t_2))$, the obstacle will be ranged again. Figure 1 (b) shows the vehicle at its new position at time $t_2$, where the obstacle is now located at $(g_x(t_2), g_y(t_2), g_z(t_2))$. The key insight to be drawn from Figure 1 is that the elevations $r_z(t_1)$ and $r_z(t_2)$, corresponding to map elements $g_z(t_1)$ and $g_z(t_2)$, are not of equal *quality*, as will be shown in the next section.

### 3.1.1 Quality of Elevation Data

The vehicle's pose is only known to a given degree of certainty, with the following mathematical representation ($x \pm \delta x, y \pm \delta y, z \pm \delta z, \Phi \pm \delta\Phi, \Theta \pm \delta\Theta, \Psi \pm \delta\Psi$). For an outdoor vehicle equipped with a differential GPS the error in the position component, $\delta x, \delta y, \delta z$, is relatively small [1] and has a minimal impact on terrain map representation as it is a small fraction of grid cell size ($\sim 10\%$). In contrast, the error in orientation can have a significant and negative impact on the quality of the elevation estimate. This error is defined as all uncertainties that affect the measurement of the orientation for a projected range and is given by $(\delta\phi, \delta\theta, \delta\psi)$. This includes:

- The orientation error associated with the vehicle's pose, $(\delta\Phi, \delta\Theta, \delta\Psi)$,
- The accuracy to which the ranging device measures the range projection, and,
- Correspondence issues related to timing of range and pose data acquisition.

Figures 2 and 3 illustrate the geometric interaction between the range projection and the orientation error for a 2-D planar example. Figure 2 shows an instance where the range projection encounters an obstacle, and Figure 3 illustrates the nominally flat ground situation. Using the small angle assumption, the error in elevation can be approximated as $\delta z = r\delta\theta$, where the angle is measured in radians. Even though $\delta\theta$ may be small, if the measured range, $r$, is sufficiently large the error in elevation, $\delta z$, is significant. The geometry of a tall vertical obstacle is most intuitive, but the small elevation change shown in Figure 3 is less obvious. In this case the pitch error contributes to both an elevation error, $\delta z$, and a location estimate that is $\delta x$ distant from the true measurement point.

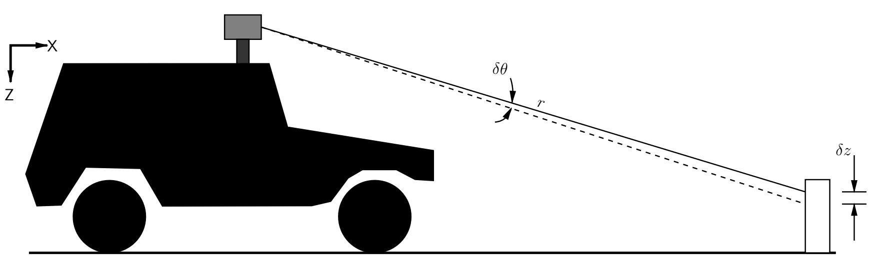


***Figure 2:*** *Geometry and Error in Pitch: Vertical Surface*

Although useful for illustrating the principles of orientation, the planar 2-D representation doesn't represent the orientation error in 3 dimensions. The effects of pitch and yaw errors are shown in Figure 4 (a). As can be seen the pitch error, $\delta\theta$, yields an elevation error of $\delta z$ and the yaw error, $\delta\psi$ produces an error of $\delta y$.

1. Example: The Novatel Span INS specifies a position error of $\pm$ 2 cm.

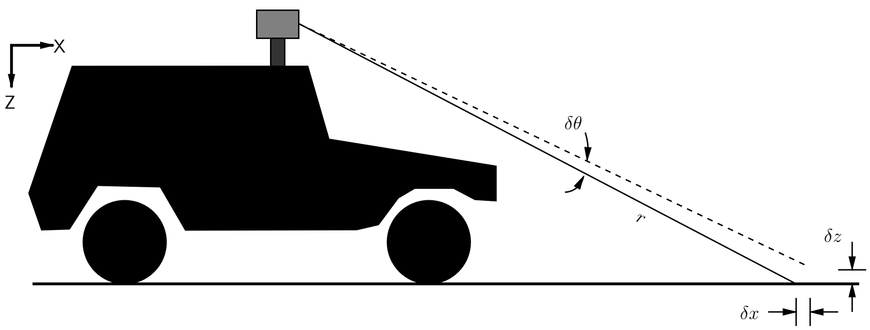


***Figure 3:*** *Geometry and Error in Pitch: Nominally Flat Surface*

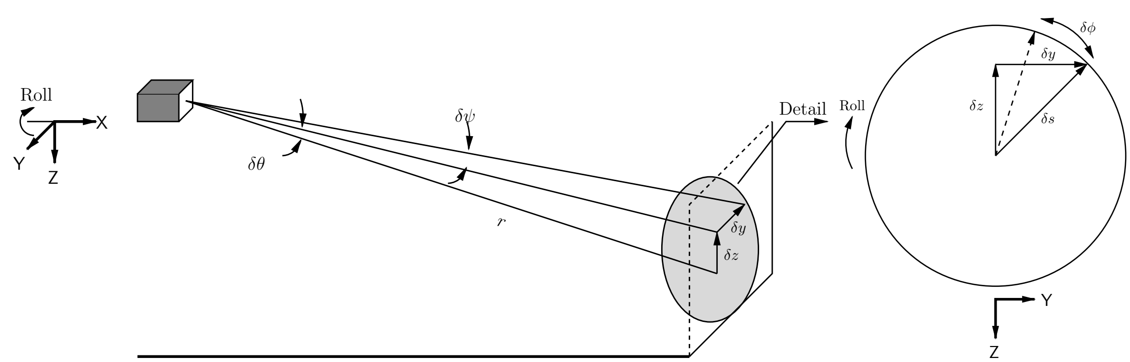


(a) 3 Dimensions

(b) Detail of Error Surface

***Figure 4:*** *Orientation Error in 3-D*

The planar representation, Figure 4 (b), illustrates the error surface, where it is obvious that a roll error, $\delta\phi$, simply rotates vector sum of the pitch and yaw errors, given by $\delta s$, around the x-axis. For this illustration a static system is assumed with the vehicle center of gravity, IMU and sensor origin all co-located together.

Given that the roll error is random, on average, it will not bias the $\delta s$ towards either the x or z components. Thus, $\delta s$ is proportional to the position error and is a function of both the range and orientation error. Building upon the idea of inverse distance weighting [36], the data quality, $q$, can be defined as proportional to the inverse of $\delta s$, as follows:

$$
\begin{aligned}
q &\propto \frac{1}{\delta s} = \frac{1}{\delta\mathbf{x} + \delta\mathbf{y}} \\
&\propto \frac{1}{\sqrt{(\delta x)^2 + (\delta y)^2}} \\
&\propto \frac{1}{\sqrt{(r\delta\theta)^2 + (r\delta\phi)^2}} \\
&\propto \frac{1}{r\sqrt{\delta\theta^2 + \delta\phi^2}}
\end{aligned} \tag{1}
$$

The above derivation is originally described in [37] and included here for clarity. This approach is only one of a number of techniques that have been proposed to address uncertainty in position provided by range data. A Kalman filter has been used in [38] to account for the uncertainty in elevation measurement, although details with respect to the sensor model and filter coefficients are not provided. Thrun et al. also noted that small errors in roll/pitch can lead to significant terrain classification error when directly analysing the point cloud for obstacles [12]. This error was modeled by a first-order Markov model where the unknown parameters were tuned via a discriminative learning algorithm and human labeled real data.

## 3.2 Terrain Map Representation

A scrollable and wrappable 2.5-D terrain map, analogous to that proposed by Kelly [26], represents the world as a grid where each element encodes the elevation. This map is globally referenced to North with the egocentric perspective being extracted when required [39]. Similar to GESTALT [29], the first and second order moment statics are collected for all range points for each map element, as is graphically illustrated in Figure 5.

| | | |
|---|---|---|
| $\bar{z}_{n+6}$ $\sigma^2_{n+6}$ | $\bar{z}_{n+7}$ $\sigma^2_{n+7}$ | $\bar{z}_{n+8}$ $\sigma^2_{n+8}$ |
| $\bar{z}_{n+3}$ $\sigma^2_{n+3}$ | $\bar{z}_{n+4}$ $\sigma^2_{n+4}$ | $\sigma^2_{n+5}$ $\sigma^2_{n+5}$ |
| $\bar{z}_{n}$ $\sigma^2_{n}$ | $\bar{z}_{n+1}$ $\sigma^2_{n+1}$ | $\bar{z}_{n+2}$ $\sigma^2_{n+2}$ |

***Figure 5:*** *Statistical Moments Stored by the Terrain Map for Fixed Grid Cells*

### 3.2.1 Weighted Statistics

The position data, derived from the range and pose, is of varying quality. In Section 3.1.1 the elevation data quality is proposed as $q$ and is a function of the inverse distance and orientation error. Thus, the statistical approach for estimating the elevation for each map element must also include a quality factor as well. Weighted statistics are well suited for this task [40]. The weighted mean and variance is given by:

$$\begin{aligned} \bar{\tau} &= \frac{\sum_{i=1}^{N} w_i \tau_i}{\sum_{i=1}^{N} w_i} \\ \sigma^2 &= \frac{\sum_{i=1}^{N} w_i (\tau_i - \bar{\tau})^2}{\sum_{i=1}^{N} w_i} \end{aligned} \tag{2}$$

$$\bar{\tau} = \frac{\sum_{i=1}^{N-1} w_i \tau_i + w_N \tau_N}{\sum_{i=1}^{N-1} w_i + w_N} \tag{3}$$

$$\sigma^2 = \frac{\sum_{i=1}^{N} w_i \sum_{i=1}^{N} w_i \tau_i^2 - \left(\sum_{i=1}^{N} w_i \tau_i\right)^2}{\left(\sum_{i=1}^{N} w_i\right)^2} \tag{4}$$

where the latter expressions are employed for computations as they are an efficient representation and ammenable to a real-time implementation:

For the purposes of updating the terrain map, the quality factor squared, $q_i$, will be used as the weighting factor, hence,

$$w_i = q_i = \frac{1}{r_i\sqrt{\delta\theta_i^2 + \delta\phi_i^2}} \tag{5}$$

In this form the weighting factor is analogous to the gain associated with a Kalman filter where it serves as an estimate of the variance. The normal format for the Kalman filter is given by [41]:

$$\hat{x}\left(t_2\right) = \hat{x}\left(t_1\right) + \frac{\sigma_{z_1}^2}{\sigma_{z_1}^2 + \sigma_{z_2}^2}\left(z_2 - \hat{x}\left(t_1\right)\right) \tag{6}$$

where $\hat{x}\left(t_1\right) = z_1$ and, $\sigma_{z_1}^2$ and $\sigma_{z_2}^2$ are the estimates of the variances. Equation 6 can be rewritten as:

$$\hat{x}\left(t_2\right) = \frac{\sigma_{z_2}^2}{\sigma_{z_1}^2 + \sigma_{z_2}^2} z_1 + \frac{\sigma_{z_1}^2}{\sigma_{z_1}^2 + \sigma_{z_2}^2} z_2 \tag{7}$$

The mean value given by weighted statistics, Equation 3, can be written as:

$$\bar{\tau} = \frac{w_1\tau_1}{w_1 + w_2} + \frac{w_2\tau_2}{w_1 + w_2} \tag{8}$$

With weighting factors $w_1 = \frac{1}{\sigma_1^2}$ and $w_2 = \frac{1}{\sigma_2^2}$ representing the variance estimates:

$$\begin{aligned}
\bar{\tau} &= \frac{\frac{\tau_1}{\sigma_1^2}}{\frac{1}{\sigma_1^2} + \frac{1}{\sigma_2^2}} + \frac{\frac{\tau_2}{\sigma_2^2}}{\frac{1}{\sigma_1^2} + \frac{1}{\sigma_2^2}} && (9) \\
&= \frac{\frac{\sigma_2^2\tau_1 + \sigma_1^2\tau_2}{\sigma_1^2\sigma_2^2}}{\frac{\sigma_1^2 + \sigma_2^2}{\sigma_1^2\sigma_2^2}} \\
&= \frac{\sigma_2^2}{\sigma_1^2 + \sigma_2^2}\tau_1 + \frac{\sigma_1^2}{\sigma_1^2 + \sigma_2^2}\tau_2 && (10)
\end{aligned}$$

Obviously, weighted statistics where the weight value is proportional to $\frac{1}{\sigma^2}$, is equivalent to the Kalman filter given in Equation 6. Under this implementation the quality factor, $q$, defined in Equation 1 is used as the Kalman filter estimated variance.

### 3.2.2 Map Statistics

Besides containing the mean elevation, $\bar{z}_n$, and variance, $\sigma_n^2$, each map element also includes the sums that allow for the computation of the weighted mean and standard deviation. Table 1 shows the sums that must be maintained:

| Count | Entry | Sum Name |
|---|---|---|
| 1 | $\bar{z}_n$ | - |
| 2 | $\sigma_n^2$ | - |
| 3 | $\sum_{i=1}^{N} w_i$ | $S_{\mathrm{w}}$ |
| 4 | $\sum_{i=1}^{N} w_i z_i$ | $S_{\mathrm{wz}}$ |
| 5 | $\sum_{i=1}^{N} w_i z_i^2$ | $S_{\mathrm{wz}^2}$ |

***Table 1:*** *Moment Statistical Entries Tallied for each Terrain map element*

From this table it can be seen that only 5 entries are required per map element. The current mean and variance are stored to eliminate the necessity to compute them from the underlying statics. This statistical map representation, in terms of the mean elevation and variance, and the means to compute these values is similar to the approach taken by Miller et al. [42]. Although the resulting statistical map representation is similar, the approach and assumptions are different. This approach starts from the Kalman filter perspective, whereas Miller et al. approach the problem from a pure statistical basis. The computing values are of importance to the global terrain map and traversability map, as will be detailed in the following sections.

## 3.3 Global Terrain Map

The global terrain map, although having no specific role to play in terms of autonomous operations, provides a human readable display that charts the robots progress. Unlike the local terrain map, which recycles elements as the map wraps and scrolls, the global terrain map is persistent and has a fixed maximum size. If and when a robot closes the loop, as shown in Figure 6, and revisits previously explored regions, the new local map data must be integrated with existing global map data.

Under the weighted statistical approach, combining data viewed at time $t_{\mathrm{u}}$ with data acquired at $t_{\mathrm{v}}$ is easily achieved. Using the weighted statistics computing forms, as given in equation 3 and 4, and summed components shown in Table 1 the estimated elevation and variance is given by:

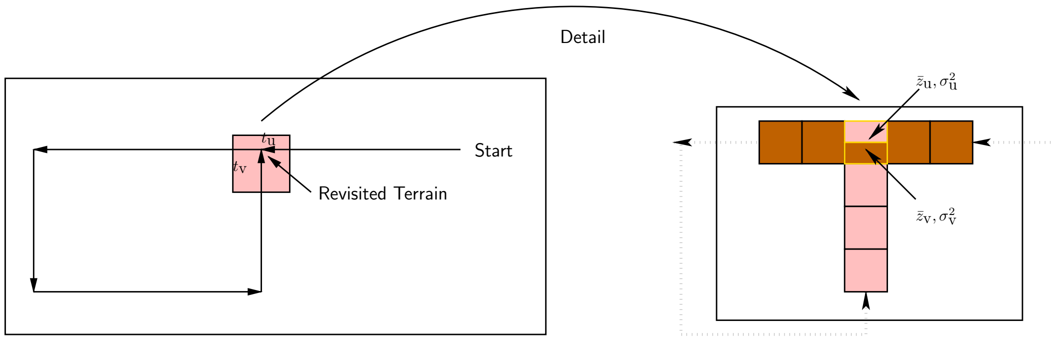


***Figure 6:*** *Terrain Map Revisiting Terrain*

$$\overline{z}_{\mathrm{v}'} = \frac{S_{\mathrm{wz}}(t_{\mathrm{u}}) + S_{\mathrm{wz}}(t_{\mathrm{v}})}{S_{\mathrm{w}}(t_{\mathrm{u}}) + S_{\mathrm{w}}(t_{\mathrm{v}})} \tag{11}$$

$$\sigma_{\mathrm{v}'}^2 = \frac{S_{\mathrm{wz}}(t_{\mathrm{u}}) \times (S_{\mathrm{wz}}(t_{\mathrm{u}}))^2 - (S_{\mathrm{wz}^2}(t_{\mathrm{u}}))^2 + S_{\mathrm{wz}}(t_{\mathrm{v}}) \times (S_{\mathrm{wz}}(t_{\mathrm{v}}))^2 - (S_{\mathrm{wz}^2}(t_{\mathrm{v}}))^2}{(S_{\mathrm{wz}}(t_{\mathrm{u}}))^2 + (S_{\mathrm{wz}}(t_{\mathrm{v}}))^2} \tag{12}$$

Where the data at $t_{\mathrm{u}}$ exists within the global terrain map and the data at $t_{\mathrm{v}}$ is supplied from the local terrain map. The combined estimation, $t_{\mathrm{v}'}$ includes the estimated elevation, $\overline{z}_{\mathrm{v}'}$, and variance, $\sigma_{\mathrm{v}'}^2$, and is stored in the global terrain map where it overwrites the previous elevation estimate.

## 3.4 Traversability Map

The data required to construct the traversability map is supplied by the terrain map. Similar to both Morphin [27] and GESTALT [28], this traversability analysis calculates the elevation difference between the a given grid and its neighbours, and then compares this value to a user defined obstacle height.

### 3.4.1 Obstacle Height

For a uniformly sampled obstacle, under conditions of no orientation error, the mean elevation is given by $\bar{h} = \frac{h}{2}$, with a variance of $\sigma^2 = \frac{h^2}{12}$. The best approximation of a terrain map's cell elevation is given by $z = \bar{h} + \frac{\sqrt{12}}{2}\sigma$, as proposed by Kelly [23]. The situation for a moving vehicle, where the sampling is random with orientation errors, is shown in Figure 7. Figure 7 (a), shows range projections onto flat terrain and Figure 7 (b) shows the situation for an obstacle.

Given that pitch has an error, the resulting elevations, $z_1, z_2, z_3$, are also in error, as shown in Figure 7. For flat terrain, a random pitch error and a large number

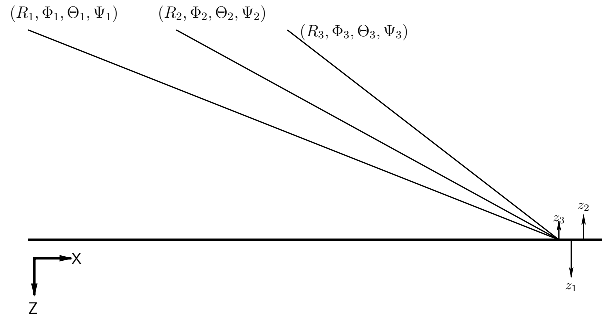


(a) Flat Terrain

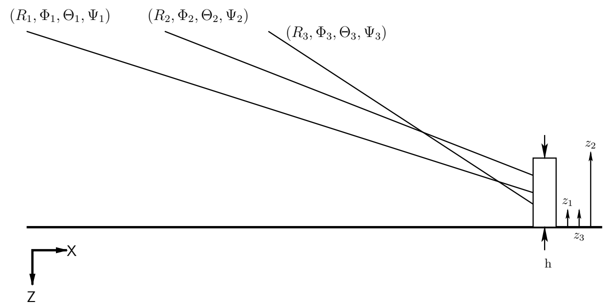


(b) Obstacle

***Figure 7:*** *Properties of Terrain Sampling*

of samples, the resulting elevation estimation, $\bar{z} = \frac{1}{N}\sum_{i=1}^{N} z_i$ is $\simeq 0$. Even though the mean elevation is near 0, the corresponding variance, $\sigma^2$, is not. Hence, the cell elevation approximation proposed by Kelly is not a suitable representation. A similar argument can be applied when an obstacle is present. In this case the cell elevation estimate, given by $\bar{z} = \frac{1}{N}\sum_{i=1}^{N} z_i$, is $\simeq \frac{h}{2}$. Thus, for a moving vehicle sampling terrain under conditions where there are orientation errors, the best approximation of a terrain map's cell elevation is $z = \bar{z} \times 2$.

### 3.4.2 Step Height Determination

The step height for each grid element in the traversability map is determined by the elevation difference between a given grid element and its four neigbours, as is illustrated in Figure 8.

For each terrain map grid element, $(\bar{z}_c, \sigma_c^2)$, where neighbours $\left[(\bar{z}_{n+1}, \sigma_{n+1}^2) \ldots (\bar{z}_{n+4}, \sigma_{n+4}^2)\right]$ exist, the maximum difference in terrain height between the center grid element and its neighbours, termed the step hazard, is given by:

$$\Delta z = \max|\bar{z}_c - \bar{z}_{n+i}| \tag{13}$$

$\Delta z \geq \Delta z_{max}$, where $\Delta z_{\max}$ is a user supplied step height threshold, implies the

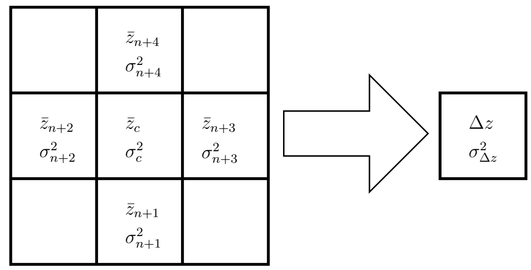


***Figure 8:*** *Step Height Determination using Adjacent Grid Cells*

presence of a traversability hazard, *i.e.* an obstacle of either positive or negative magnitude.

A heuristic step height comparison is not statistical and, thus, does not fully exploit the available data. To predict an obstacle's presence the data quality must also be incorporated. In its general form the variance is estimated as follows, where the weighting factor is given by equation 5:

$$\begin{aligned} \sigma^2 &= \frac{\sum_{i=1}^{n} w_i \times (z_i - \bar{z})^2}{\sum_{i=1}^{n} w_i} \\ &= \frac{\sum_{i=1}^{n} w_i \times \sum_{i=1}^{n} w_i z_i^2 - \left(\sum_{i=1}^{n} w_i z_i\right)^2}{\left(\sum_{i=1}^{n} w_i\right)^2} \end{aligned} \tag{14}$$

For the traversability map the variance, associated with the step height, must be determined. The elevation error, around the true elevation, is assumed to be normally distributed, hence the step height error is also normal. The variance for the step hazard, using the weighted statistics computing forms from Table 1, is as follows:

$$\sigma^2_{\Delta z} = \frac{S_{\mathrm{wz}}(c) \times S_{\mathrm{wz}^2}(c) - (S_{\mathrm{wz}}(c))^2 + S_{\mathrm{wz}}(n+i) \times S_{\mathrm{wz}^2}(n+i) - (S_{\mathrm{wz}}(n+i))^2}{(S_{\mathrm{wz}}(c))^2 + (S_{\mathrm{wz}}(n+i))^2} \tag{15}$$

#### 3.4.3 Probability of an Obstacle

The first stage of the traversability analysis determined the step height, $\Delta z$, and the corresponding variance, $\sigma^2_{\Delta z}$ for each grid element in the terrain map. The second stage uses these values, along with the user defined obstacle height, to determine the probability of flat terrain, given by $P(T)$. Normally distributed orientation errors have been assumed. Under this assumption it follows that the elevation variance will also be normally distributed. With the standard normal distribution, $\mu = 0$ and $\sigma = 1$, distance from the mean is described by *z-scores* ($\zeta$), as given in the following section.

#### 3.4.3.1 Probability Density Function

The probability density function (PDF) best illustrates the obstacle detection technique. For the normal distribution the z-*score* is given by:

$$\begin{aligned} \zeta &= \frac{x \pm \mu}{\sigma} \\ &= \frac{\Delta z \pm \Delta z_{max}}{\sigma} \end{aligned} \tag{16}$$

Assume the laser ranges nominally flat terrain, as shown in Figure 1, with a measured elevation and variance $(\bar{z}_i, \sigma_i^2)$. Then, for all grid elements $i$, $\bar{z}_i \simeq 0$, as the terrain is flat. Hence the step hazard, $\Delta z$ defined by equation (13), is also $\simeq 0$ and the *z-scores* reduce to:

$$\zeta_i = \frac{\Delta z \pm \Delta z_{max}}{\sigma_i} \simeq \frac{\pm \Delta z_{max}}{\sigma_i} \tag{17}$$

The corresponding probability density function (PDF) is shown in Figure 9. The area $T_i$ represents the probability of all hazards less than $\Delta z_{max}$ and greater than -$\Delta z_{max}$. As this is the probability of flat terrain, the probability of a hazard is given by $\mathrm{P}(O) = 1 - \mathrm{P}(T)$, represented by the area $2H_i$.

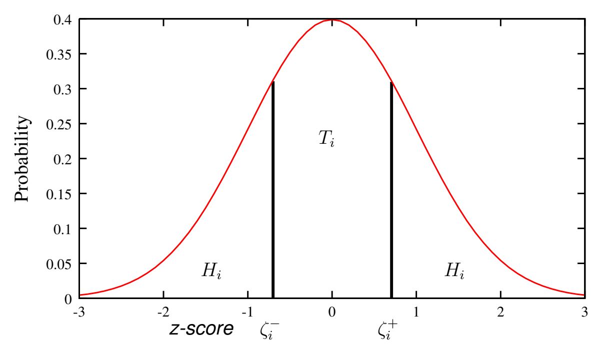


***Figure 9:*** *Probability Density Function $(\bar{z}_i, \sigma_i)$*

When the data quality is better, the variance decreases. Consider the situation in which $\sigma_j^2 \ll \sigma_i^2$ where its corresponding PDF shown in Figure 10. Again the *z-scores* for $(\bar{z}_j, \sigma_j^2)$ are given by $\zeta_j = \pm \Delta z_{max}/\sigma_j$, since for flat terrain $\bar{z}_j \simeq 0$. Once again,

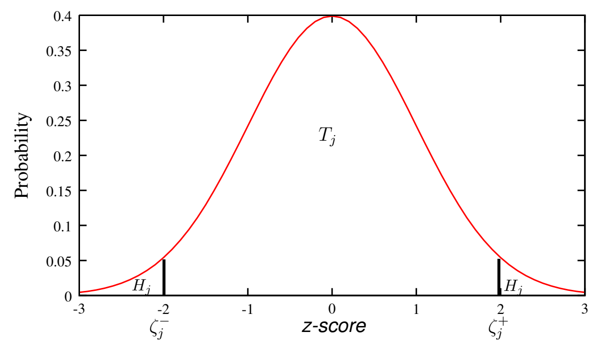


***Figure 10:*** *Probability Density Function* $(\bar{z}_j, \sigma_j)$

the area $T_j$ under the curve represents the probability of flat terrain and the area $2H_j$ corresponds to the probability of a step hazard. As expected the area $2H_j$ is much less than the area $2H_i$, indicative of an increased confidence that the terrain is indeed flat.

The presence of an obstacle results in an expanded range of elevation values. In the case where the mean elevation equals the step hazard threshold, as given by $\bar{z}_k = \Delta z_{\max}$, the *z-scores* are given by:

$$\zeta_k = \frac{\bar{z}_k \pm \Delta z_{\max}}{\sigma_k}$$

Hence, $\zeta_k^+ = \dfrac{2\Delta z_{\max}}{\sigma_k}$ and $\zeta_k^- = 0$. In Figure 11 the area $T_k$ represents the probability of flat terrain and the summed area $H_k + H_k^1$ is the hazard probability.

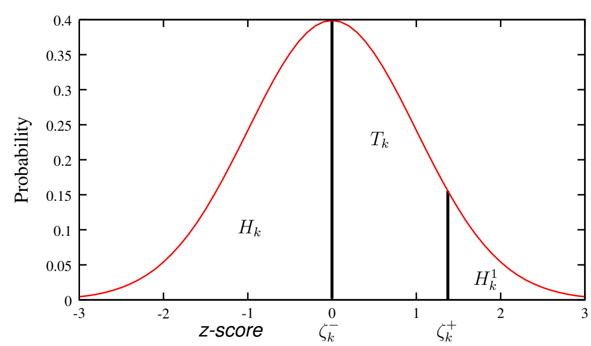


***Figure 11:*** *Probability Density Function* $(\bar{z}_k, \sigma_k)$

The step height threshold, $\Delta z_{\max}$, and the variance, $\sigma^2$, are the same for both Figures 9 and 11. Hence, the magnitude $\zeta_{\text{diff}} = \left(\zeta_i^+ - \zeta_i^-\right) = \left(\zeta_k^+ - \zeta_k^-\right)$ remains constant.

As can be seen in Figures 9 and 11, the introduction of a mean elevation, $\bar{z}_k$, has simply shifted flat terrain region position's under the PDF curve.

#### 3.4.3.2 Cumulative Density Function

Although the PDFis a useful tool for illustrating the statistics of probabilistic obstacle detection, the cumulative density function (CDF) is more appropriate for implementation. The CDF, $F_X(x) = \mathrm{P}(X \leq x)$, is the probability that a random variable X will have a value less than or equal to $x$; in terms of the PDF, $f(x)$,

$$F(x) = \int_{-\infty}^{x} f(\tau) d\tau$$

The probability of flat terrain is given as follows:

$$\begin{aligned} \mathrm{P}(T) &= F(\zeta^+) - F(\zeta^-) \\ &= \mathrm{P}(\zeta^- \leq X \leq \zeta^+) \\ &= \int_{\zeta^-}^{\zeta^+} f(\tau)\, d\tau \end{aligned} \tag{18}$$

where $f(x)$ is the normal PDF, $\zeta^+ = {}^{(\Delta z + \Delta z_{\max})}/_{\sigma}$ and $\zeta^- = {}^{(\Delta z - \Delta z_{\max})}/_{\sigma}$. $\mathrm{P}(T)$ represents the probability of flat terrain and corresponds to the area under the PDF between the limits $\zeta^+$ and $\zeta^-$, as shown in Figures 9, 10 and 11. The CDF, shown in Figure 12, represents the PDFintegration, thus, the probability is read directly from the vertical axis.

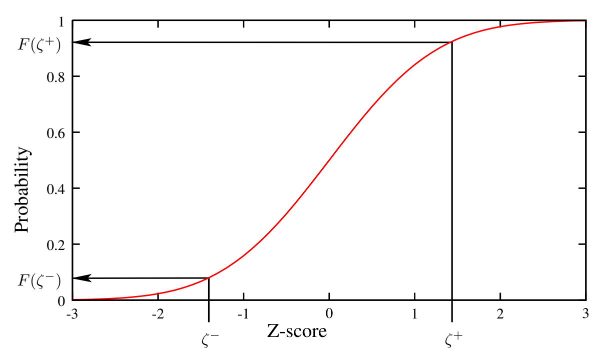


***Figure 12:*** *Cumulative Density Function ($\pm\zeta$)*

### 3.4.4 Probabilistic Traversability Map

Following the steps described in the preceding sections, each valid terrain map grid element can be mapped into a traversability map, where each grid element is assigned the probability of an obstacle, P($O$). Figure 13 illustrates the mapping between the terrain map and the traversability map, with the terrain on the left and the traversability map located on the right.

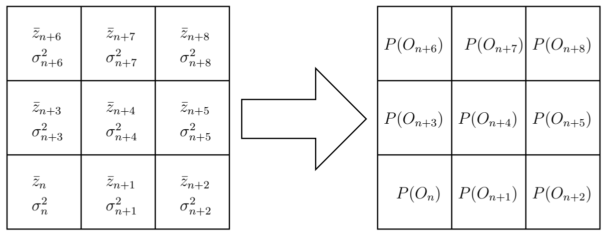


***Figure 13:*** *Probabilistic Traversability Map*

#### 3.4.4.1 Advantages

The probabilistic approach incorporates the range data quality and this is crucial as the quality of a range datum varies with the distance of its corresponding terrain patch from the vehicle and the vehicle's orientation accuracy. Thus, the probabilistic approach automatically accounts for the effects of elevation changes, resulting from orientation errors and long range measurements, hence this research is congruent with and reinforces the probabilistic terrain analysis approach used by the Stanley robot [35].

#### 3.4.4.2 Interpretation

In a traditional, heuristic-based traversability map each grid element was either occupied, free or unknown. In contrast, a probabilistic traversability map is open to a number of interpretations:

- If traversability is examined at a specified confidence level, the grid elements of the resulting map are in the traditional occupied, free or unknown format. Additionally, the selected confidence level can be influenced by outside factors such as the vehicle being located on a known road or the fact the location corresponds to unstructured terrain.
- The obstacle probability, P($O$), can be interpreted as traversal cost associated with the given grid element. Thus, traversability map explorations sum the total traversal cost for a selected route through the map.
- The traversability map could be a hybrid, where each grid element has an associated traversal cost up to a given probability, $\mathrm{P}_{\mathrm{max}}(O)$. Grid elements with probability $\mathrm{P}_{\mathrm{i}}(O) \geq \mathrm{P}_{\mathrm{max}}(O)$ would be deemed impassible.

### 3.4.5 Rollover Hazard

Obstacles are not the only hazards faced by a UGV. Steep slopes can be a stability hazard where the vehicle is at the risk of a rollover. Two approaches have been proposed to quantify the rollover hazard, *area-based* and *path-based*. The *area-based* technique, exemplified by Morphin, evaluates all possible terrain patches [27]. When the rollover risk is sensitive to the vehicle's approach direction then a *path-based* approach is more appropriate. Similar to Ranger [43], this paper proposes a *path-based* rollover hazard technique. To quantify this hazard the UGV's wheel locations are projected onto the terrain map for each selected traversal path. These four wheel patches, illustrated by the brown squares in Figure 14 (a), provide the data that allows the determination of the plane shown in pink.

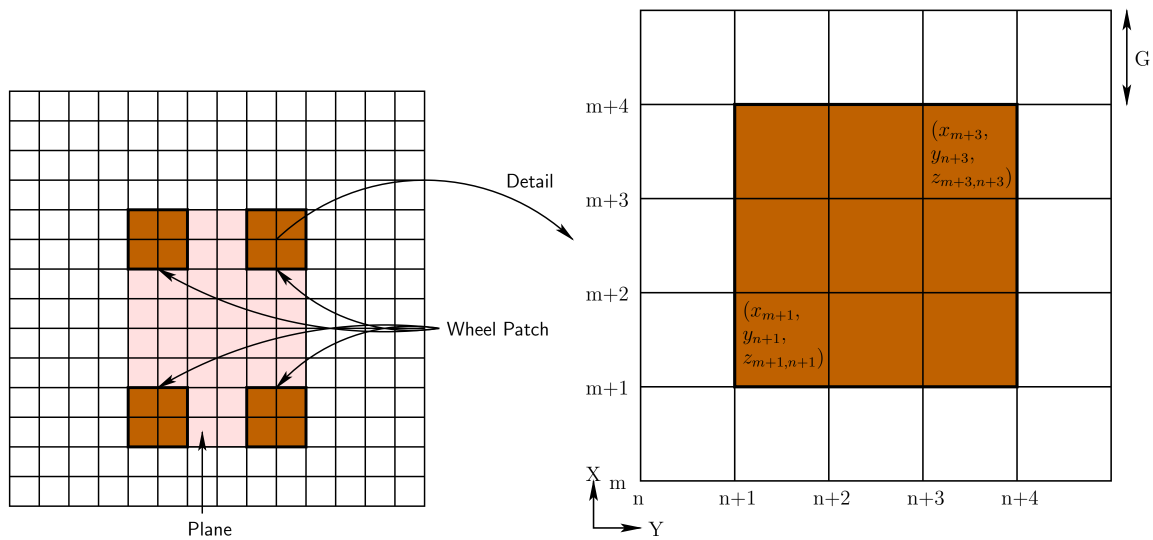


(a) Terrain Map (b) Wheel Patch

***Figure 14:*** *Vehicle Plane*

The wheel patch detail, shown in Figure 14 (b), encompasses a number of terrain map elements, dependent on both the wheel and grid size. Each grid element is represented by a point $P_i(x_m, y_n, z_{m,n})$:

$$x_m = G \times \left(m + \frac{1}{2}\right) \quad (19)$$

$$y_n = G \times \left(n + \frac{1}{2}\right) \quad (20)$$

where $G$ is the grid size, $x_m$ is the element's center in the $\mathbf{X}$ direction, $y_n$ is the element's center in $\mathbf{Y}$ direction and $z_{m,n}$ is the weighted elevation from the terrain map. The weighted elevation ensures that the underlying data *goodness* is factored into the elevation determination.

#### 3.4.5.1 Fitting a Plane

Any plane can be represented by an equation of the form:

$$Ax + By + Cz + D = 0 \tag{21}$$

The terrain map elements, $P_i$, under each of the four wheel patches create a vector of points that lie on the plane.

$$\begin{gathered} P_0(x_0, y_0, z_0) \\ P_1(x_1, y_1, z_1) \\ \vdots \\ P_Q(x_Q, y_Q, z_Q) \end{gathered}$$

Substituting the point, for all $Q$ points, into the equation of a plane yields:

$$\begin{aligned} Ax_0 + By_0 + Cz_0 + D &= 0 \\ Ax_1 + By_1 + Cz_1 + D &= 0 \\ &\vdots \\ Ax_Q + By_Q + Cz_Q + D &= 0 \end{aligned} \tag{22}$$

Represented in matrix format:

$$\mathbf{b} = \mathbf{A}\mathbf{x} \tag{23}$$

where $\mathbf{b}$ is:

$$\mathbf{b} = \begin{bmatrix} 0 \\ 0 \\ \vdots \\ 0 \end{bmatrix} \tag{24}$$

and $\mathbf{A}$ is:

$$\mathbf{A} = \begin{bmatrix} x_0 & y_0 & z_0 & 1 \\ x_1 & y_1 & z_1 & 1 \\ \vdots & \vdots & \vdots & \vdots \\ x_Q & y_Q & z_Q & 1 \end{bmatrix} \tag{25}$$

and $\mathbf{x}$ is:

$$\mathbf{x} = \begin{bmatrix} A \\ B \\ C \\ D \end{bmatrix} \tag{26}$$

The coefficients, $\mathbf{x}$, can then be determined using a best fit solution, in matrix format [44]:

$$\mathbf{x} = \mathbf{P}\mathbf{b} \tag{27}$$

where the projection matrix $\mathbf{P}$ is defined as:

$$\mathbf{P} = \left(\mathbf{A}^T\mathbf{A}\right)^{-1}\mathbf{A}^T \tag{28}$$

Hence:

$$\mathbf{x} = \left(\mathbf{A}^T\mathbf{A}\right)^{-1}\mathbf{A}^T\mathbf{b} \tag{29}$$

Solving these simultaneous equations using an ordinary least squares fit to yield the $(A, B, C, D)$ coefficients of the plane can be accomplished by various methods [2].

#### 3.4.5.2 Quality of the Parameter Estimate

The least squares residuals are given by:

$$\hat{\varepsilon} = \mathbf{b} - \mathbf{A}\mathbf{x} \tag{30}$$

2. Specifically Lapack DGELS is used to solve these simultaneous equations.

The least squares estimator for variance, $\sigma^2$, is:

$$\begin{aligned} \sigma^2 &= \frac{1}{Q}\hat{\boldsymbol{\varepsilon}}^2 \\ &= \frac{1}{Q}\hat{\boldsymbol{\varepsilon}}^T\hat{\boldsymbol{\varepsilon}} \\ &= \frac{1}{Q}\left(\mathbf{b}-\mathbf{A}\mathbf{x}\right)^T\left(\mathbf{b}-\mathbf{A}\mathbf{x}\right) \end{aligned} \tag{31}$$

where $Q$ is the number of points used for the plane fit.

#### 3.4.5.3 Estimating the Rollover Hazard

The terrain map used for hazard avoidance is ego-centric [39], thus the $\mathbf{X}$ direction is perpendicular to the bumper and the $\mathbf{Y}$ direction is parallel, as shown in Figure 15 (a).

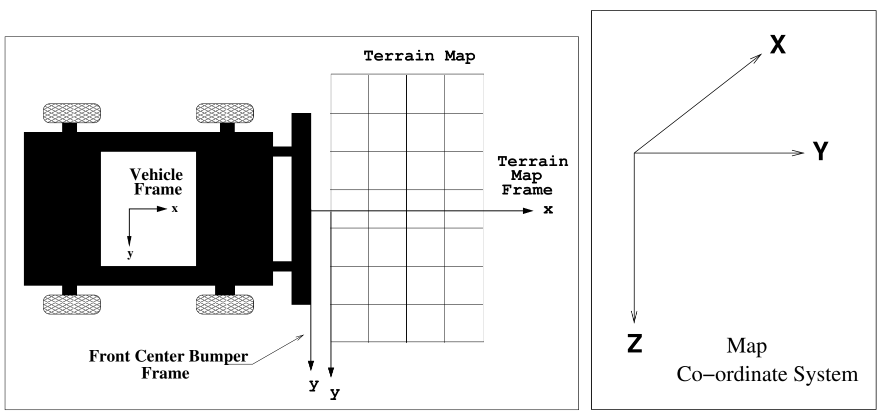


(a) Ego-centric Map Frame (b) Map Co-ordinate System

***Figure 15:*** *Ego-centric Map Frame and Co-ordinate System*

Vehicle roll is defined as about the $\mathbf{X}$ axis, at the center of gravity, hence only $(y, z)$ components influence it. Determining roll of the plane is straight forward. Using the plane's equation and the point $P_r(0, 1, z_r)$ allows for the calculation of a line parallel to the bumper, where $z_r$ is:

$$z_r = \frac{-D - B}{C} \tag{32}$$

A vector from the front center bumper, to the point $P_r$, is given by $\mathbf{u} = \hat{j} + z_r\hat{k}$. For flat terrain there is no elevation change, thus the $\hat{k}$ component is zero, and the vector is given by $\mathbf{v} = \hat{j}$. Given two vectors, $\mathbf{u}_c = a_1\hat{j} + b_1\hat{k}$ and $\mathbf{v}_c = a_2\hat{j} + b_2\hat{k}$, the angle between the vectors is given by:

$$\cos\phi = \frac{a_1 a_2 + b_1 b_2}{|\mathbf{u}_c|\,|\mathbf{v}_c|} \tag{33}$$

For the vector in the plane, $\boldsymbol{u}$ and the vector of flat terrain, $\boldsymbol{v}$, $a_1 = 1$, $b_1 = z_r$, $a_2 = 0$ and $b_2 = 1$:

$$\begin{aligned} \cos\phi &= \frac{z_r}{\sqrt{1^2 + z_r^2} \times \sqrt{1^2}} \\ &= \frac{z_r}{\sqrt{1 + z_r^2}} \end{aligned} \tag{34}$$

Solving for the roll angle $\phi_r$ yields:

$$\phi_r = \cos^{-1}\left(\frac{\frac{-D-B}{C}}{\sqrt{1 + \left(\frac{-D-B}{C}\right)^2}}\right) \tag{35}$$

### 3.4.6 Probability of Roll Hazard

The probability of a roll hazard is determined in a manner similar to that presented for the probability of an obstacle. Although a maximum roll angle, $\Delta r_{max}$, is defined it is not directly compared to the calculated plane roll, $\phi_r$. As was implemented for obstacles, calculated roll is assumed to have a normal distribution and the area representing *not* a roll is determined. For the normal distribution the z-*score* is given by:

$$\zeta = \frac{\phi_r \pm \Delta r_{max}}{\sigma} \tag{36}$$

where plane fit quality is given by $\sigma^2$, as determined by Equation 32. The probability of *not* a roll hazard, $\mathrm{P}(\dot{r})$, is given by:

$$\mathrm{P}(\dot{r}) = F(\zeta^+) - F(\zeta^-) \tag{37}$$

The roll hazard, $\mathrm{P}(r)$, is then given as $\mathrm{P}(r) = 1 - \mathrm{P}(\dot{r})$.

## 3.5 Global Traversability Map

The global traversability map remembers all obstacles encountered within a X by Y region and is crucial for long range path planning. Similar to the global terrain map, the global traversability map must fuse current and previous data under situations where terrain is revisited, as is illustrated in Figure 16. Once again weighted statistics are the basis for the fusion, but in this case the probability of obstacles are weighted by their corresponding variances. The weighted computing formula presented in equation 10 is the means of performing this fusion. Where the probability of an obstacle is given by $\tau_i = \mathrm{P}(O)_i = 1 - \mathrm{P}(T)_i$ and the variance is given by $\sigma_i^2$, then for the grid elements shown in the map of Figure 16 is:

$$\tau_v' = \frac{\sigma_v^2}{\sigma_u^2 + \sigma_v^2}\tau_u + \frac{\sigma_u^2}{\sigma_u^2 + \sigma_v^2}\tau_v$$

Hence the probability of an obstacle, for the revisited grid element, is the variance weighted sum of the existing probabilities in a manner that is analogous to a Kalman filter.

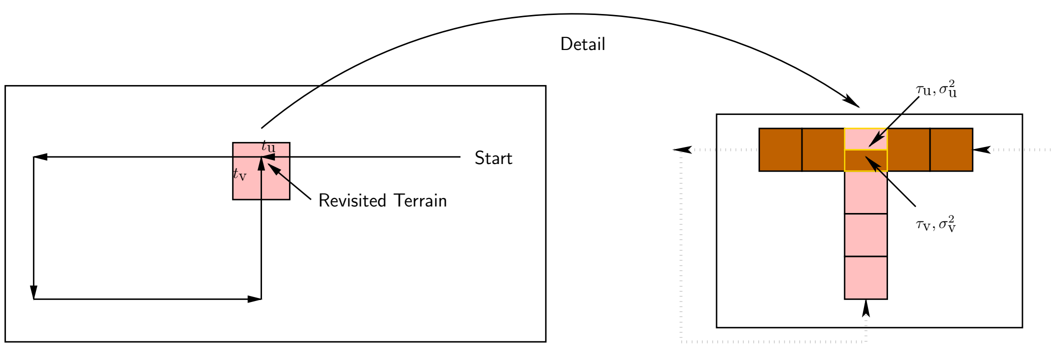


***Figure 16:*** *Traversability Map Revisiting Terrain*

# 4 Results

## 4.1 Implementation

All world representation software and all supporting software was developed under the Miro framework [45, 46]. The Miro framework inherently supports data logging and playback. Additionally, its flexible event-based implementation allows the user to seamlessly switch between real world, simulated and logged data.

### 4.1.1 Simulation Environment

A dedicated Miro interface allows the Gazebo simulator [47] to directly publish/receive Miro based events. The Gazebo interface currently supports range data and the vehicle pose. Additionally it receives steering and speed commands, which are passed along to Gazebo, thus, commanding the simulated vehicle.

### 4.1.2 Raptor UGV

Experiments in the real world were conducted using the Raptor UGV shown in Figure 17. The Raptor features: A Velodyne HDLaser, a Point Grey BumbleBee XB3 Stereo camera, the Novatel HG1700 Span INS, and, a dual Quad Core Intel Xeon CPU at 2.66 GHz.

***Figure 17:*** *Raptor Unmanned Ground Vehicle*

## 4.2 Simulations

Simulations are an excellent tool for designing, debugging and testing algorithmic implementation. Although the *perfect* data sets don't accurately represent the real world, they allow for the systemic investigation of an algorithm's performance. For this research, the simulated Raptor UGV uses two fixed angle SICK lasers, one at 12° below the horizon and second laser mounted at 20°. Both lasers are mounted

1.7 m above the ground plane. Additionally, the Gazebo simulator provides data that simulates the performance of the Novatel HG1700 Span IMU. Figure 18 (a) and (c) show simulated terrain maps where elevation is denoted by colour. As can be seen the world is flat, as denoted by the green area, and the walls are shown in blue.

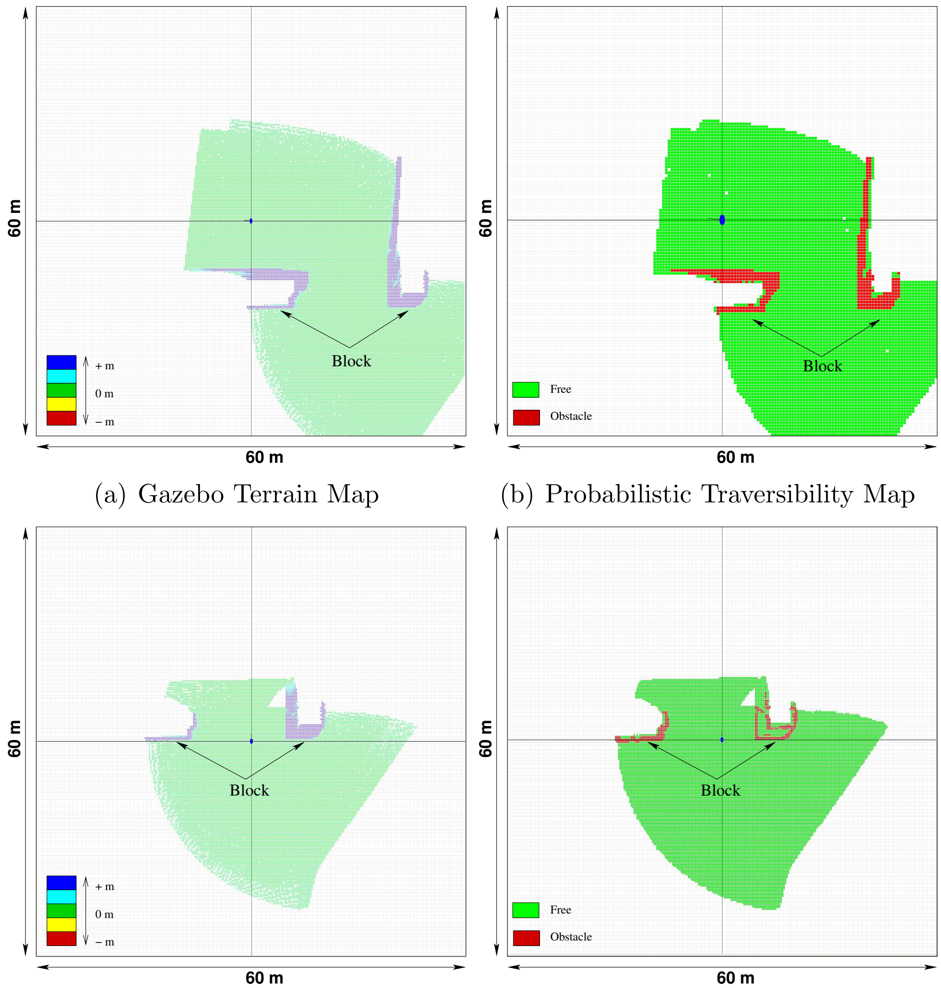


(a) Gazebo Terrain Map (b) Probabilistic Traversability Map

(c) Gazebo Terrain Map (d) Probabilistic Traversability Map

***Figure 18:*** *Traversability Maps using Simulated Gazebo Data*

The corresponding probabilistic traversability maps are shown in Figure 18 (b) and (d). For these maps, traversible terrain is shown in green and obstacles are denoted by red. Not surprisingly the simulations, providing *perfect* data where the ground is absolutely flat, the obstacles are vertical, and both the range and pose data is error free, yield accurate terrain and traversability maps. For the traversability analysis the probability of an obstacle is set to 80%.

The cost of traversal, shown in Figure 19, corresponds to maps (c) and (d) in Figure 18. For this map blue denotes a low cost and red represents a high traversal cost. The transition from flat to elevated obstacles is evident from the green/yellow colours located near the obstacles.

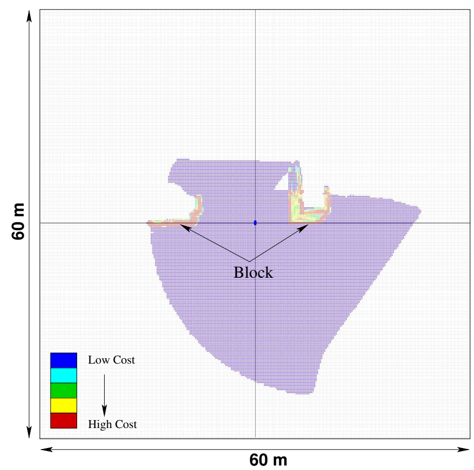


***Figure 19:*** *Cost of Traversal Map using Simulated Gazebo Data*

A Gazebo simulation also provided the data for a comparison between a heuristic traversability analysis and the probabilistic implementation. Gazebo created a terrain map using simulated data with random roll/pitch errors up to 1°. The terrain was analysed for traversability using a heuristic approach [48] and the technique detailed by this paper. This analysis attempted to identify obstacles denoted by a step height threshold, $\Delta z_{\max}$, of 0.35 m. As is evident by observation, the probabilistic traversability analysis shown in 20(a), with the probability of an obstacle set to 90%, produced a traversability map that better identified the true block obstacle than did the heuristic map shown in 20(b). Additionally, when the probabilistic map, 20(a), and heuristic map, 20(b), are visually compared, it is obvious that the probabilistic approach was significantly less affected by the random orientation errors as fewer grid elements were misidentified as obstacles.

### 4.2.1 Simulations with Errors in Orientation

Simulations were performed to quantify the performance of the weighted statistical terrain map. For the terrain maps shown in Figure 21 the error in pitch and roll was uniformly distributed between 0° and 1°.

The variance between the ground plane and the terrain map was determined for the area where the two lasers have overlapping coverage. This corresponds to approximately 4.0 m in front of the vehicle and 10 m on either side of the vehicle's center

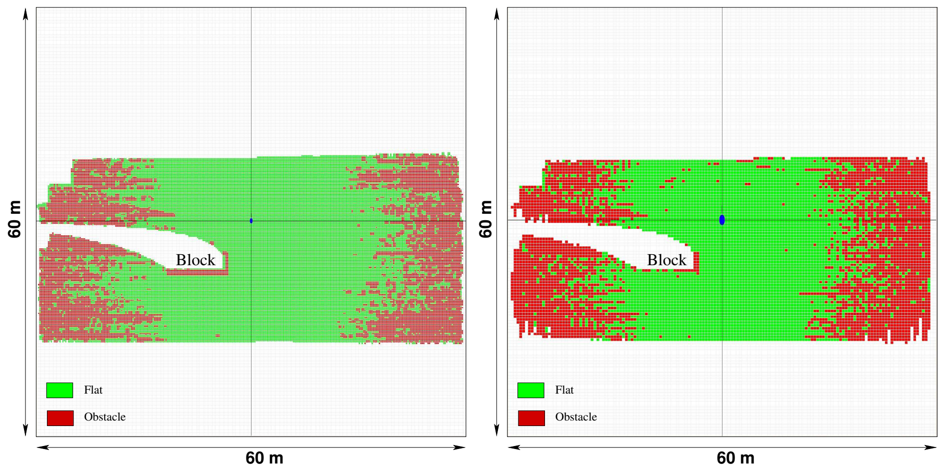

(a) Probabilistic Traversability Map (b) Heuristic Traversability Map

***Figure 20:*** *Traversability Maps using Simulated Gazebo Data*

line. Figure 21 (a) shows the terrain map that results when a simple average is used. In Figure 21 (b) the results for a weighted average are presented. For the simple averaging approach the standard deviation was 36.1 mm. When the technique was switched to weighted statistics the standard deviation dropped by just over 1 mm to 34.9 mm. Not surprisingly, visually there is little apparent difference between the two maps where the terrain in predominately flat and portrayed by the green color.

A second data set was acquired with the pitch and roll error increased to 2°. As seen in Figure 22 this larger roll and pitch error results in a terrain map where elevation variations are visually apparent as given by the red, yellow and blue discolorations mainly evident at the map margins. Within the region of analysis, the map based upon standard statistics, while visually quite similar to the weighted statistics map, seems to show slightly more color variation.

The standard deviation from the ground plane was 86.1 mm when simple averaging statistics were employed. For weighted statistics the standard deviation from the ground plane decreased to 83.1 mm. In both experiments, the configuration of the shallowest laser, at an angle of 12° below the horizon, limited the advantages of the weighted statistics approach, since the shallow laser provided a lookahead distance of only 8 m.

The final experiment used a laser at the standard 20°, with the shallow laser set to an angle of 3.8°. Once again the roll and pitch error was specified as uniform between 0° and 1°. As is obvious in Figure 23, the roll and pitch error significantly affects the range data from the shallow angle laser. In the region under analysis there are no obvious visible differences in appearance. The analysis of the standard deviation

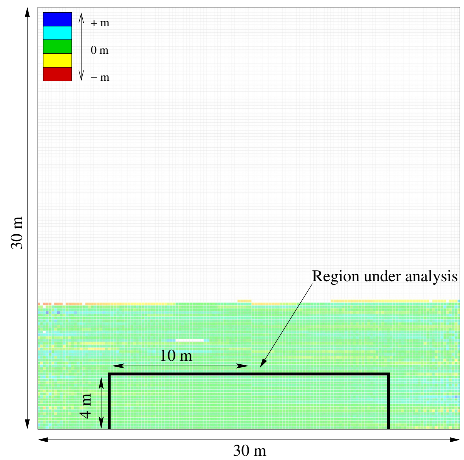

(a) Standard Statistics

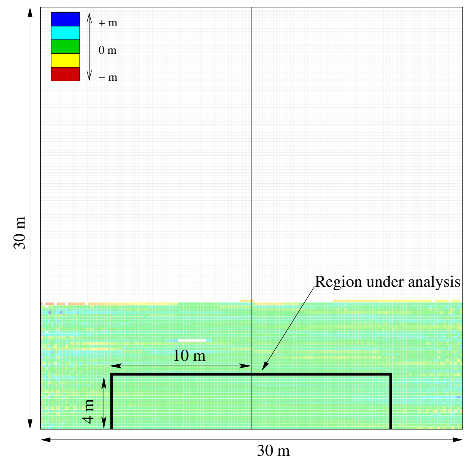

(b) Weighted Statistics

***Figure 21:*** *Terrain Maps using Simulated Data: Roll/Pitch error up to* 1°

from the ground plane reveals a value of 70.7 mm for standard statistics and a mean of 59.5 mm for weighted statistics.

### 4.2.2 Simulations with Obstacle Detection

Simulated data using lasers mounted at 20° and 12°, with no orientation error, and with a uniform roll/pitch between 0° and 1° added to the orientation, was used for the experiments on obstacle detection. Figure 24 (a), shows the terrain map produced when there is no error in orientation. In Figure 24 (a) both obstacles are identified by the elevation changes, as shown in blue. Both the terrain and traversability maps are $60 \times 60$ metres, with the terrain map grid size set to 200 mm and a traversability map grid size of 400 mm.

As described in Section 3.4.3, obstacle detection is probabilistic hence the detection process can be assigned a confidence level. Experiments were performed where obstacles were identified at four confidence levels: 85%, 90%, 95% and 99%. The step height threshold was 350 mm for all experiments. The traversability map, Figure 24(b), clearly identifies the obstacles at a 95% confidence level. Table 2 provides the number of obstacles within the traversability map, for each of the specified confidence levels.

Figure 25 shows the traversability map results for the 99%, 90% and 85% confidence levels. As is obvious from these figures, increasing the confidence level not only suppresses false-positives, but also suppresses the identification of real obstacles.

The experiment was then repeated with the row and pitch errors defined as a random

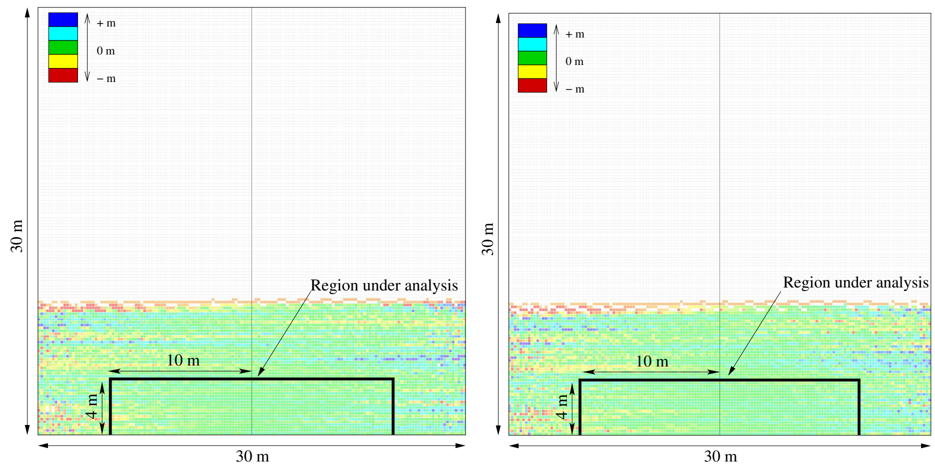


(a) Standard Statistics (b) Weighted Statistics

***Figure 22:*** *Terrain Maps using Simulated Data: Roll/Pitch error up to 2°*

| Confidence Level | Grid Cells Identified as Obstacles |
|---|---|
| 99% | 33 |
| 95% | 85 |
| 90% | 132 |
| 85% | 172 |

***Table 2:*** *Number of Obstacles Detected vs. Confidence Level*

variable, normally distributed, with a standard deviation of 1°. Figure 26 (a) shows the terrain map produced under these conditions. As can be seen, one obstacle is evident, but the second obstacle is partially obscured within the noise of the map. The traversability map, at the 95% confidence level, is shown in Figure 26 (b). As can be seen, it only identifies a single obstacle, and the map fringes are populated with *phantom* obstacles.

The terrain map was also analysed for obstacles at the 99%, 90% and 85% confidence intervals, as shown in Figure 27. From these figures it is obvious that the confidence level has a significant impact on the resulting traversability map. For a high noise environment, increasing the confidence level acts as a filter that suppresses spurious obstacles. In these experiments increasing the confidence level resulted in a more reliable identification of obstacle-free terrain and a clearer delineation of true obstacles. Thus, the obstacle near the map's center becomes more evident as the confidence level increases. Although this statistical approach provides solid results, it is unable to reliably detect the obstacle on the top left side of the map. The roll and pitch noise, in tandem with the long range of near 30 m effectively obscures the obstacle.

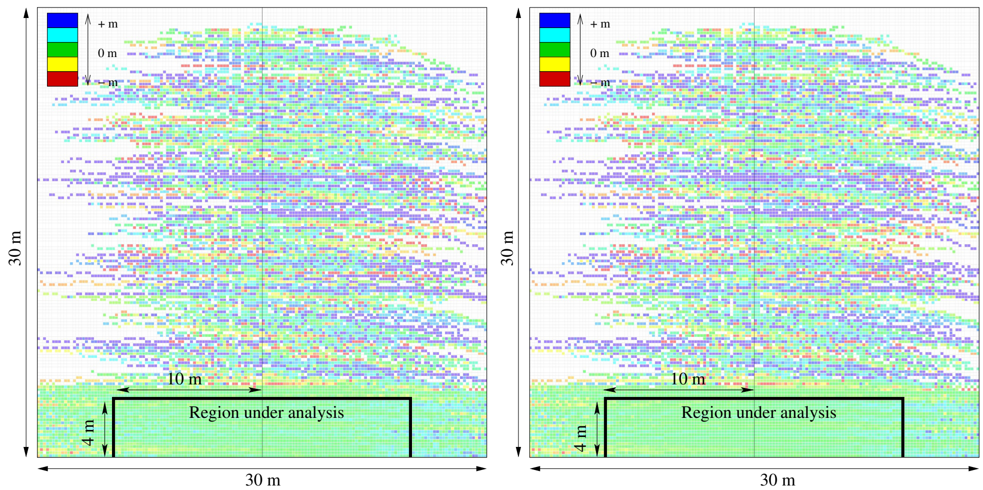


(a) Standard Statistics (b) Weighted Statistics

***Figure 23:*** *Simulated Data with an Extended Lookahead Distance*

Table 3 identifies the number obstacles identified at each respective confidence level. The table and traversability maps illustrate how effectively this statistical approach can suppress *phantom* obstacles, even in the presence of data with significant errors.

| Confidence Level | Grid Cells Identified as Obstacles |
|---|---|
| 99% | 1178 |
| 95% | 2317 |
| 90% | 3071 |
| 85% | 3646 |

***Table 3:*** *Number of Obstacles Detected vs. Confidence Level, with a Roll/Pitch Error*

For comparison purposes, the same simulated data was feed into a GESTALT inspired traversability analysis [48]. Again, the step hazard value was set to 350 mm. Figure 28 shows the traversability that results when there is no pitch and roll errors applied. Under these circumstances the map labels 1278 elements as obstacles. Figure 28(b), shows the traversability maps that results when the orientation error is applied. For this analysis the map labeled 4178 grid elements as obstacles.

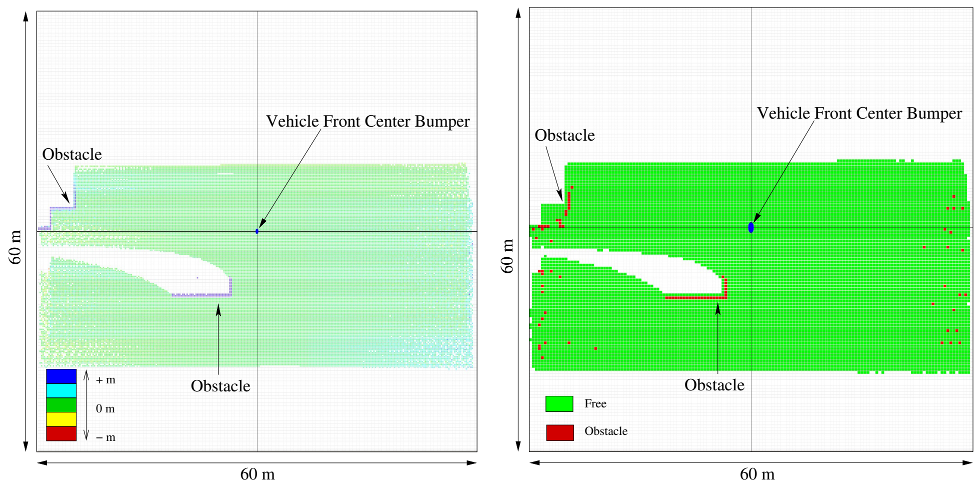


(a) Terrain Map (b) Traversibility Map, 95% Confidence

***Figure 24:*** *Terrain and Traversibility Maps with no Orientation Error*

## 4.3 Field Trials

Using the Raptor UGV, field data was logged while the traversing the local environment. Figure 29 shows the terrain for the first scene.

Figure 30(a) shows the terrain map of the environment. Once again colour denotes elevation with red indicating low regions, green representing zero elevation and blue denotes elevated regions. The road, ditches and exit are clearly evident. Applying the probabilistic obstacle detection technique to the real world terrain map yields the traversability map shown in Figure 30(b). For this traversability map the threshold probability of an obstacle is specified as 90%. As is evident, the map identifies the road and ditch margins. The cost of traversal map, shown in Figure 30(c), highlights the probability of encountering a traversability hazard. In this figure red represents a high traversal cost and the colors yellow, green, light blue through to dark blue represent descending traversal costs. As can be seen, the traversal cost map follows the terrain map's form, while clearly identifying traversable and non-traversable regions.

A second data set was analysed in which the environment featured a fence line, building and vehicles. Figure 31 (a) presents a snapshot as seen from the Raptor UGV looking forward, where a building is evident to the left, a building is partially in view to the right, and a vehicle is directly ahead of the Raptor UGV. The corresponding terrain map, Figure 31 (b), clearly shows the building situated on both sides of the Raptor UGV. The traversability map, given in Figure 31 (c), identifies both buildings, as well as a fence line and two vehicles as obstacles. In the terrain map, Figure 31 (a), two buildings, two vehicles, a fence line and flat terrain can be identified. For this experiment the obstacle probability was again specified as 90%.

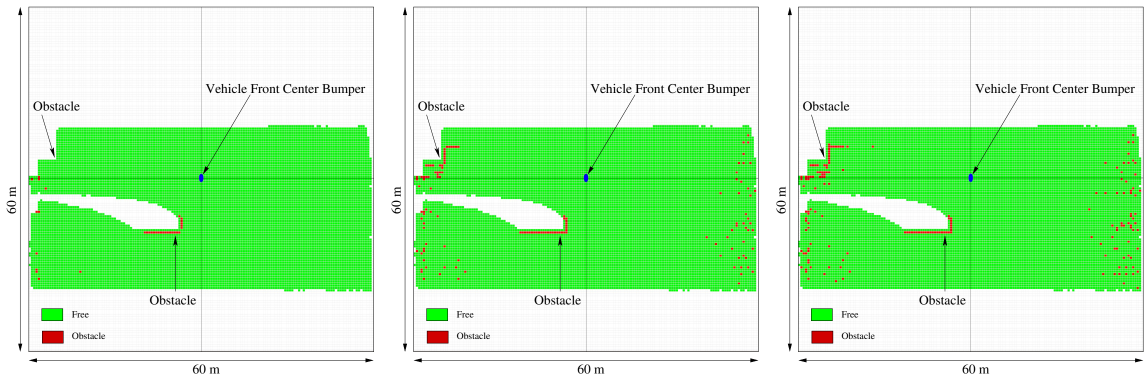


(a) 99% Confidence (b) 90% Confidence (c) 85% Confidence

***Figure 25:*** *Traversibility Maps with no Orientation Error*

Finally, the cost of traversal map is given in Figure 32. As with the case for both the terrain map and the traversability map, the cost of traversal map clearly identifies flat terrain as low cost (given in blue) and higher cost regions are denoted in shades of yellow to red. The correspondence between obstacles and the region associated with a higher traversal cost are evident.

# 5 Conclusions

This paper presents a statistical technique that identifies the presence of obstacles. The probabilistic traversability map, derived from the underlying statistical terrain map, automatically accounts for and adjusts to terrain map reliability. Obstacles measured at a longer range, or with a significant orientation error, yield terrain map elements with larger variance. The traversability map, when determining the step hazard, uses estimated elevation variance to provide a statistical estimate of the terrain's traversability.

This technique has been tested with both simulated and real world data. In simulation where the range data was corrupted by a specific amount, the probabilistic traversability approach was an improvement over the previous purely heuristic approach. With real world data the probabilistic traversability map reliably identified impediments to traversal. It was tested with various semi-structured environments and in each case the result was a faithful representation of the real world. Although traversability maps have historically taken an occupancy grid format, this research has opened a new avenue for traversability map interpretation. Given that the map represents the probability of an obstacle, it can also be viewed as the cost of traversal. Using this perspective route planners could avoid higher cost regions, corresponding to a higher probability of an obstacle, even though the region is not specifically tagged

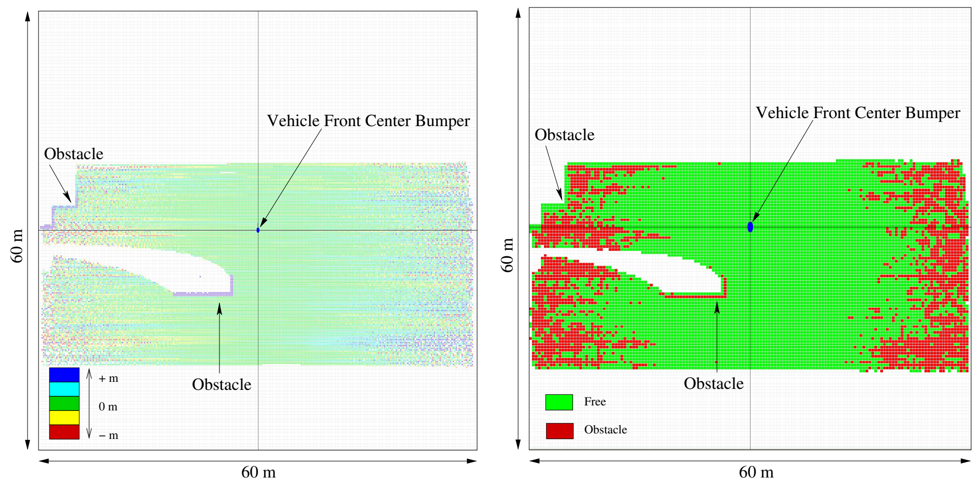


(a) Terrain Map (b) Traversibility Map, 95% Confidence

***Figure 26:*** *Traversibility Map, Simulated Environment, with Obstacles and a Roll/Pitch Error*

as non-traversable.

# 6 Future Work

This statistical approach is amenable to other types of traversability analysis. Vehicle roll over is another significant hazard where, traditionally, purely heuristic approaches have been the norm. This statistical approach has been adapted to predict the roll over hazard, but experiments to quantify its performance have yet to be conducted.

Additionally, it would be highly desirable to compare the presented technique's performance against other traversability implementations, especially the probabilistic technique used by the Stanley UGV. Unfortunately such comparisons are difficult to perform given that this would require an independent implementation of the "probabilistic terrain analysis" approach, which is not a simple and straightforward task.

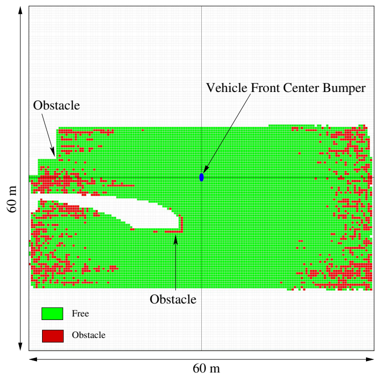


(a) 99% Confidence

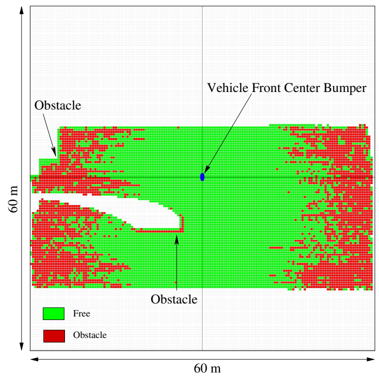


(b) 90% Confidence

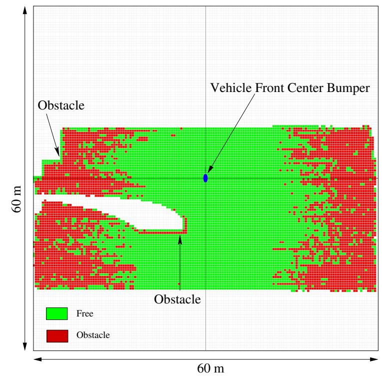


(c) 85% Confidence

***Figure 27:*** *Traversibility Maps resulting from Differing Confidence Levels*

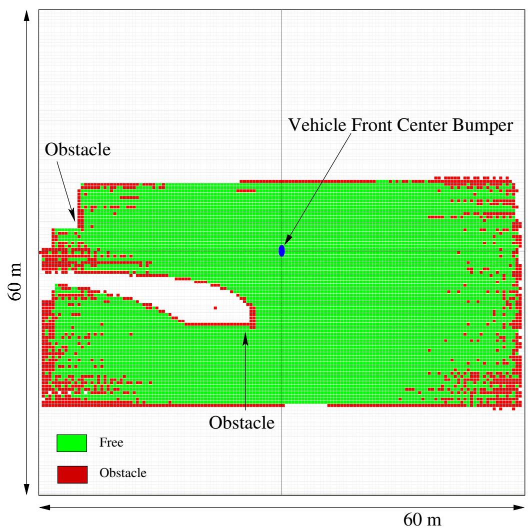


(a) No Roll/Pitch Error

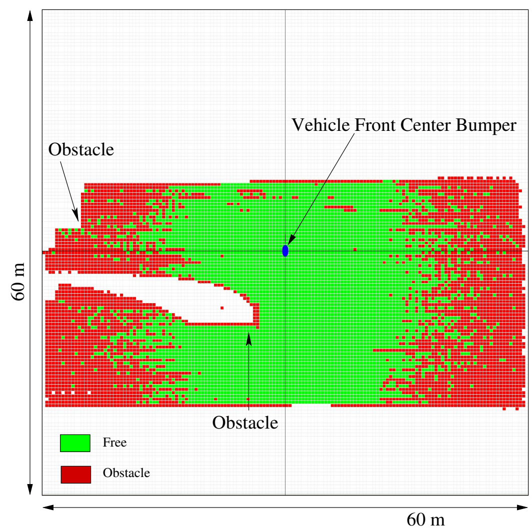


(b) Roll/Pitch Error

***Figure 28:*** *Traversibility Maps resulting from the GESTALT Approach*

***Figure 29:*** *Environment of the First Trial*

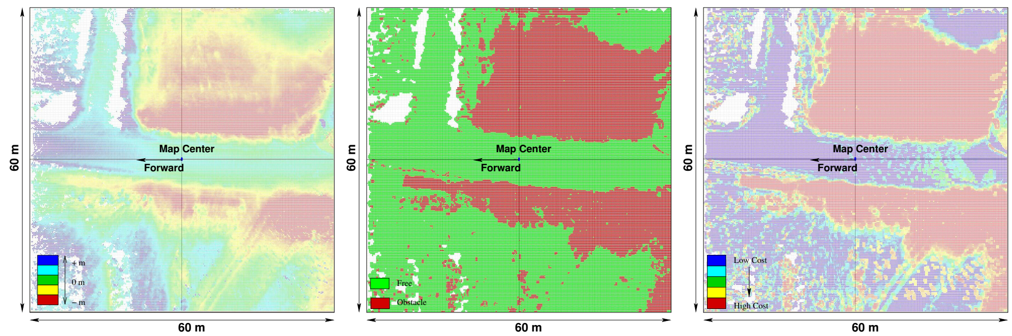


(a) Terrain Map (b) Probabilistic Traversability Map (c) Traversal Cost Map

***Figure 30:*** *Traversability Maps*

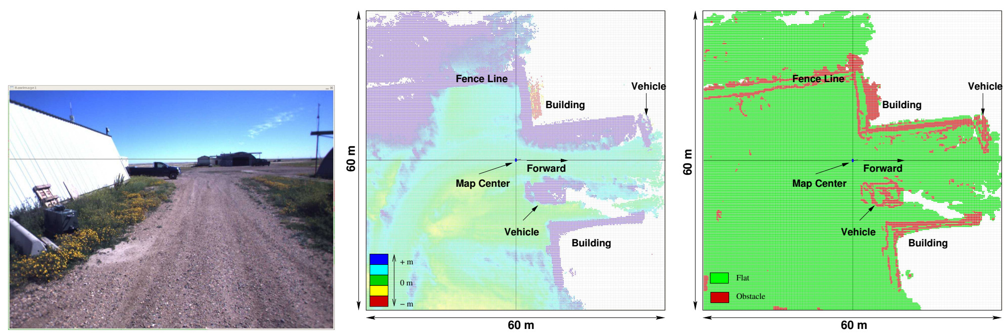


(a) Environment of the Second Trial (b) Terrain Map (c) Probabilistic Traversability Map

***Figure 31:*** *Traversability Maps*

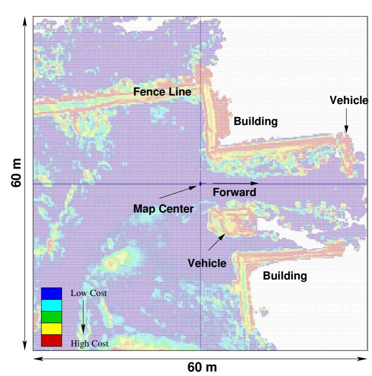


***Figure 32:*** *Traversal Cost Map*

# References


[1] Moravec, H. (1980), Obstacle Avoidance and Navigation in the Real World by a Seeing Robot Rover, In *tech. report CMU-RI-TR-80-03, Robotics Institute, Carnegie Mellon University & doctoral dissertation, Stanford University*, Number CMU-RI-TR-80-03.

[2] Nilsson, N. J. (1984), Shakey The Robot, (Technical Report 323) AI Center, SRI International, 333 Ravenswood Ave., Menlo Park, CA 94025.

[3] Moravec, H. (1983), The Stanford Cart and the CMU Rover, *Proceedings of IEEE*, 71(7), 872–884.

[4] Thompson, A. (1977), The Navigation System of the JPL Robot, In *Proceedings of the International Joint Conference on Artificial Intelligence*, pp. 749–757, IJCA-5.

[5] Moravec, H. and Elfes, A. E. (1985), High Resolution Maps from Wide Angle Sonar, In *Proceedings of the 1985 IEEE International Conference on Robotics and Automation*, pp. 116 – 121.

[6] Borenstein, J. and Koren, Y. (1989), Real-Time Obstacle Avoidance for Fast Mobile Robots, *IEEE Transactions on Systems, Man and Cybernetics*, 19(5), 1179–1187.

[7] Borenstein, J. and Koren, Y. (1991), The Vector Field Histogram - Fast Obstacle Avoidance for Mobile Robots, *IEEE Transactions on Robotics and Automation*, 7(3), 535–539.

[8] Hebert, M. and Krotkov, E. (1992), 3D measurements from imaging laser radars: how good are they?, *Image Vision Comput.*, 10(3), 170–178.

[9] Matthies, L. and Grandjean, P. (1994), Stochastic performance, modeling and evaluation of obstacle detectability with imaging range sensors, *Robotics and Automation, IEEE Transactions on*, 10(6), 783–792.

[10] Matthies, L., Litwin, T., Owens, K., Rankin, A., Murphy, K., Coombs, D., Gilsinn, J., Hong, T., Legowik, S., B., M. N., and Yoshimi (1998), Performance evaluation of UGV obstacle detection with CCD/FLIR stereo vision and LADAR, In *Intelligent Control (ISIC), 1998. Held jointly with IEEE International Symposium on Computational Intelligence in Robotics and Automation (CIRA), Intelligent Systems and Semiotics (ISAS), Proceedings*, pp. 658–670.

[11] Ye, C. and Borenstien, J. (2002), Characterization of a 2-D Laser Scanner for Mobile Robot Ostacle Negotiation, In *Proceedings of the IEEE International Conference on Robotics and Automation*, pp. 2512–2518, Washington, DC, USA.

[12] Thrun, S., Montemerlo, M., Dahlkamp, H., Stavens, D., Aron, A., Diebel, J., Fong, P., Gale, J., Halpenny, M., Hoffmann, G., Lau, K., Oakley, C., Palatucci, M., Pratt, V., Stang, P., Strohband, S., Dupont, C., Jendrossek, L.-E., Koelen, C., Markey, C., Rummel, C., van Niekerk, J., Jensen, E., Alessandrini, P., Bradski, G., Davies, B., Ettinger, S., Kaehler, A., Nefian, A., and Mahoney, P. (2006), Stanley: The Robot That Won the DARPA Grand Challenge, *Journal of Field Robotics*, 23(9), 661–692.

[13] Shan, J. and Toth, C. K., (Eds.) (2008), Topographic Laser Ranging and Scanning: Principles and Processing, CRC.

[14] Weingarten, J. W., Gruener, G., and Siegwart, R. (2004), A State-of-the-art 3D Sensor for Robot Navigation, In *Proceedings of the IEEE/RSJ International Conference on Intelligent Robots and Systems*, Sendai, Japan.

[15] Kortenkamp, D. and Bonasso, R. (1998), Artificial Intelligence and Mobile Robots: Case Studies of Successful Robot Systems, 1st ed, AAAi Press.

[16] Elfes, A. (1989), Using Occupancy Grids for Mobile Robot Perception and Navigation, *Computer*, 22(6), 46–57.

[17] Collins, T., Collins, J., and Ryan, C. (2007), Occupancy Grid Mapping: An Empirical Evaluation, In *Proceedings of the 15th Mediterranean Conference on Control and Automation*, Athens, Greece.

[18] Olin, K. and Tseng, D. (1991), Autonomous Cross-Country Navigation: an Integrated Perception and Planning System, *IEEE Expert*, 6, 16–30.

[19] Thorpe, C., Hebert, M., Kanade, T., and Shafer, S. (1988), Vision and Navigation for the Carnegie-Mellon Navlab, *IEEE Transactions on Pattern Analysis and Machine Intelligence*, 10(3), 362–373.

[20] Hebert, M., Caillas, C., Krotkov, E., Kweon, I., and Kanade, T. (1989), Terrain Mapping for a Roving Planetary Explorer, In *Proceedings of the IEEE International Conference on Robotics and Automation*, pp. 997–100.

[21] Bares, J., Hebert, M., Kanade, T., Krotkov, E., Mitchell, T., Simmons, R., and Whittaker, W. R. L. (1989), Ambler: An Autonomous Rover for Planetary Exploration, *IEEE Computer*, 22(1), 18–26.

[22] Kweon, S. and Kanade, T. (1992), High-Resolution Terrain Map from Multiple Sensor Data, *IEEE Transactions on Pattern Analysis and Machine Vision*, 14(2), 278–292.

[23] Kelly, A. J. (1997), An Approach to Rough Terrain Autonomous Mobility, In *International Conference on Mobile Planetary Robots*, Santa Monica.

[24] Ponce, J. and Brady, M. (1985), Toward a Surface Primal Sketch, In *International Conference of Robotics and Automation*.

[25] Hebert, M. and T. Kanade, T. (1986), Outdoor Scene Analysis Using Range Data, In *Proceedings of the IEEE International Conference on Robotics and Automation*, pp. 1426–1432, San Francisco.

[26] Kelly, A. J. (1995), Predictive Control Approach to the High-Speed Cross-Country Autonomous Navigation Problem, Ph.D. thesis, Carnegie Mellon University, Pittsburg, Pa.

[27] Simmons, R., Henrikson, L., Chrisman, L., and Whelan, G. (1996), Obstacle avoidance and safeguarding for a lunar rover, *AIAA Forum on Advanced Developments in Space Robotics*.

[28] Biesiadecki, J., Maimone, M. W., and Morrison, J. (2001), The Athena SDM Rover: a Testbed for Mars Rover Mobility, *International Symposium on Artificial Intelligence, Robotics and Automation in Space i-SAIRAS '01*.

[29] Goldberg, S., Maimone, M., and Matthies, L. (2002), Stereo Vision and Rover Navigation Software for Planetary Exploration, *IEEE Aerospace Conference Proceedings*.

[30] Chang, T., Legowik, S., and Abrams, M. N. (1999), Concealment and Obstacle Detection for Autonomous Driving, In *Proceedings of the Robotics & Applications 1999 Conference*, pp. 28–30.

[31] Manduchi, R., Castano, A., Talukder, A., and Matthies, L. (2005), Obstacle Detection and Terrain Classification for Autonomous Off-Road Navigation, *Autonomous Robots*, 18, 81–102.

[32] Vandapel, N., Huber, D., Kapuria, A., and Hebert, M. (2004), Natural Terrain Classification using 3-D Ladar Data, In *IEEE International Conference on Robotics and Automation*.

[33] Hebert, M. and Vandapel, N. (2003), terrain classification techniques from ladar data for autonomous navigation, In *Collaborative Technology Alliances conference*.

[34] Dima, C. and Hebert, M. (2005), Active Learning For Outdoor Obstacle Detection, In *Proc. Science and Systems I.*

[35] Thrun, S., Montemerlo, M., and Aron, A. (2006), Probabilistic terrain analysis for high-speed desert driving, In Sukhatme, G., Schaal, S., Burgard, W., and Fox, D., (Eds.), *Proceedings of the Robotics Science and Systems Conference*, Philadelphia, PA.

[36] Hugentobler, M. (2004), Terrain modelling with triangle based free form surface, Ph.D. thesis, Department of Geography, University of Zurich.

[37] Broten, G. and Collier, J. (2006), Continuous Motion, Outdoor, 2 1/2D Grid Map Generation using an Inexpensive Nodding 2-D Laser Rangefinder, In *Proceedings of the 2006 IEEE International Conference on Robotics and Automation*, Number 2006-061, pp. 4240–4245, Orlando, Fl.

[38] Pfaff, P. and Burgard, W. (2005), An Efficient Extension of Elevation Maps for Outdoor Terrain Mapping, In *FSR*, pp. 195–206.

[39] Broten, G., Monckton, S., Mackay, D., and Collier, J. (2007), World Representations for Unmanned Ground Vehicles, In Grant R. Gerhart, D. W. G., Charles M. Shoemaker, (Ed.), *Proceedings of SPIE, Unmanned Systems Technology IX*, Vol. 6561, p. 11, Orlando, FL.

[40] Freund, J. E. (1982), Modern Elementary Statistics, Sixth edition ed, Prentice-Hall.

[41] Maybeck, P. S. (1979), Stochastic models, estimation, and control, Vol. 141 of *Mathematics in Science and Engineering*, Academic Press.

[42] Miller, I., Lupashin, S., Zych, N., Moran, P., Schimpf, B., Nathan, A., and Garcia, E. (2006), Cornell university's 2005 DARPA grand challenge entry, *Journal of Field Robotics*, 23(8), 625–652.

[43] Kelly, A. (1994), A Partial Analysis of the High Speed Autonomous Navigation, (Technical Report CMU-RI-TR-94-16) Robotics Institute, Pittsburgh, PA.

[44] Strang, G. (1980), Linear Algebra and its Applications, Ch. Projections onto Subspaces and Least Squares Approximation, Academic Press.

[45] Utz, H., Sablatnog, S., Enderle, S., and Kraetzschmar, G. (2002), Miro - Middleware for Mobile Robot Applications, *IEEE Transactions on Robotics and Automation*, 18, 493–497.

[46] Broten, G., Mackay, D., S., M., and Collier, J. (2009), The Robotics Experience: Beyond Components and Middleware, *IEEE Robotics and Automation Magazine*, 16(2008-227), 46–54.

[47] Koenig, N. and Howard, A. (2004), Design and Use Paradigms for Gazebo, An Open-Source Multi-Robot Simulator, pp. 2149–2154.

[48] Collier, J., Broten, G., and Giesbrecht, J. (2006), Traversibility Analysis for Unmanned Ground Vehicles, (DRDC Suffield TM 2006-175) Defence R&D Canada – Suffield, P.O. Box 4000, Station Main, Medicine Hat, Albe.

This page intentionally left blank.

**DOCUMENT CONTROL DATA**

(Security markings for the title, abstract and indexing annotation must be entered when the document is Classified or Protected.)

| | |
|---|---|
| 1. ORIGINATOR (The name and address of the organization preparing the document. Organizations for whom the document was prepared, e.g. Centre sponsoring a contractor's report, or tasking agency, are entered in section 8.)<br><br>Defence R&D Canada – Suffield<br>PO Box 4000, Medicine Hat, AB, Canada<br>T1A 8K6 | 2a. SECURITY MARKING (Overall security marking of the document, including supplemental markings if applicable.)<br><br>UNCLASSIFIED<br><br>2b. CONTROLLED GOODS<br><br>(NON-CONTROLLED GOODS)<br>DMC A<br>REVIEW: GCEC JUNE 2010 |

3. TITLE (The complete document title as indicated on the title page. Its classification should be indicated by the appropriate abbreviation (S, C or U) in parentheses after the title.)

End-to-End Statistical World Representations: Terrain Mapping to Traversability Analysis

4. AUTHORS (Last name, followed by initials – ranks, titles, etc. not to be used.)

Broten, G. S.; Collier, J. A.; Mackay, D. J.; Monckton, S. P.; Digney, B. L.

| 5. DATE OF PUBLICATION (Month and year of publication of document.) | 6a. NO. OF PAGES (Total containing information. Include Annexes, Appendices, etc.) | 6b. NO. OF REFS (Total cited in document.) |
|---|---|---|
| November 2013 | 58 | 48 |

7. DESCRIPTIVE NOTES (The category of the document, e.g. technical report, technical note or memorandum. If appropriate, enter the type of report, e.g. interim, progress, summary, annual or final. Give the inclusive dates when a specific reporting period is covered.)

Technical Report

8. SPONSORING ACTIVITY (The name of the department project office or laboratory sponsoring the research and development – include address.)

Defence R&D Canada – Suffield
PO Box 4000, Medicine Hat, AB, Canada T1A 8K6

| 9a. PROJECT OR GRANT NO. (If appropriate, the applicable research and development project or grant number under which the document was written. Please specify whether project or grant.) | 9b. CONTRACT NO. (If appropriate, the applicable number under which the document was written.) |
|---|---|
| | |

| 10a. ORIGINATOR'S DOCUMENT NUMBER (The official document number by which the document is identified by the originating activity. This number must be unique to this document.) | 10b. OTHER DOCUMENT NO(s). (Any other numbers which may be assigned this document either by the originator or by the sponsor.) |
|---|---|
| DRDC Suffield TR 2013-060 | |

11. DOCUMENT AVAILABILITY (Any limitations on further dissemination of the document, other than those imposed by security classification.)

Unlimited

12. DOCUMENT ANNOUNCEMENT (Any limitation to the bibliographic announcement of this document. This will normally correspond to the Document Availability (11). However, where further distribution (beyond the audience specified in (11)) is possible, a wider announcement audience may be selected.)

Unlimited

13. ABSTRACT (A brief and factual summary of the document. It may also appear elsewhere in the body of the document itself. It is highly desirable that the abstract of classified documents be unclassified. Each paragraph of the abstract shall begin with an indication of the security classification of the information in the paragraph (unless the document itself is unclassified) represented as (S), (C), or (U). It is not necessary to include here abstracts in both official languages unless the text is bilingual.)


Robot navigation requires reliable perception that generates an appropriate world representation. This is especially true for outdoor, unstructured or semi-structured environments where impediments to traversal are more complex than simple insurmountable obstacles. Such environments include negative features, such as ditches, as well as positive features in the form of sloping rises, that may constitute obstacles to traversal. These features must be captured by the world representation in a manner that properly handles the uncertainty associated with range data and the vehicle pose. An analysis of this representation can then extract traversable and non-traversable regions. Finally, this processing must proceed in near real-time in order to allow the robot to travel at reasonable speeds. This paper presents a statistical approach that starts with a 2.5D terrain map, follows through to the traversability analysis, and continues to the ancillary global terrain and traversability representations. At all stages the data's statistical relevance is carried forward and incorporated into the analysis. This technique has been verified using simulations and heavily exercised on a physical robot under real world conditions. These experiments have revealed that the proposed approach performs well, producing both terrain and traversability maps that adequately portray their environment.

La navigation par robot exige une perception fiable selon laquelle une représentation appropriée du monde est produite. Cela est particulièrement vrai pour les environnements extérieurs, non structurés ou semi-structurés où les entraves au déplacement sont plus complexes que de simples obstacles insurmontables. Ces environnements comportent des particularités négatives, comme des fossés, ainsi que des particularités positives se présentant sous la forme de pentes montantes, qui peuvent gêner le déplacement. Ces particularités doivent être saisies lors de la représentation du monde d'une manière qui permette de gérer l'incertitude associée aux données télémétriques et à la pose d'un véhicule. Une analyse de cette représentation permet ensuite d'extraire les régions où des obstacles gênent le déplacement et où ce dernier peut se faire librement. Enfin, ce traitement doit se faire en temps quasi-réel afin de que le robot puisse se déplacer à des vitesses raisonnables. Le présent document décrit une approche statistique établie d'après une carte topographique 2.5D; il traite ensuite de l'analyse des entraves au déplacement et se poursuit par des représentations auxiliaires globales concernant le terrain et le déplacement sans gêne. À toutes les étapes, la pertinence des données sur le plan statistique est reprise et intégrée à l'analyse. Cette technique a été vérifiée au moyen de simulations et a été mise à l'épreuve de manière intensive sur un robot physique dans des conditions du monde réel. Ces expériences ont révélé que l'approche proposée fonctionne bien; elle produit des cartes du terrain et des entraves au déplacement qui décrivent de manière adéquate l'environnement.


14. KEYWORDS, DESCRIPTORS or IDENTIFIERS (Technically meaningful terms or short phrases that characterize a document and could be helpful in cataloguing the document. They should be selected so that no security classification is required. Identifiers, such as equipment model designation, trade name, military project code name, geographic location may also be included. If possible keywords should be selected from a published thesaurus. e.g. Thesaurus of Engineering and Scientific Terms (TEST) and that thesaurus identified. If it is not possible to select indexing terms which are Unclassified, the classification of each should be indicated as with the title.)


self-supervised, on-line, real-time, learning, adaptive, inferred geometry, terrain mapping